Cell Reports

Article

SHMT2-mediated mitochondrial serine metabolism drives 5-FU resistance by fueling nucleotide biosynthesis

Graphical abstract

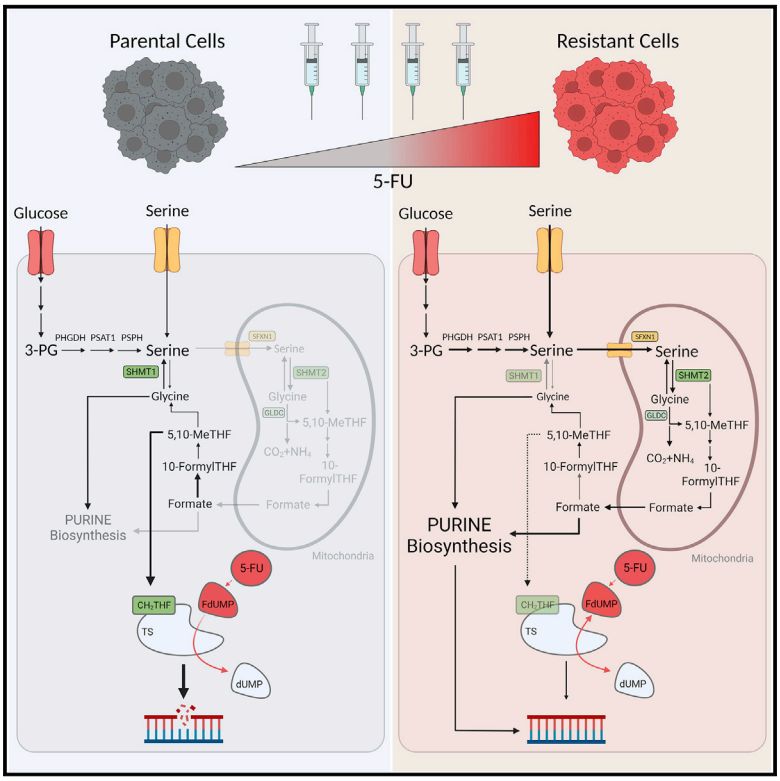

Highlights

- Serine metabolism is a key driver of 5-FU acquired resistance in CRC
- Affecting serine availability impairs DNA damage response in 5-FU-resistant cells
- Mitochondrial compartmentalization of serine metabolism sustains 5-FU resistance
- Targeting mitochondrial serine metabolism is effective in overcoming 5-FU resistance

Authors

Erica Pranzini, Elisa Pardella, Livio Muccillo, ..., Oliver D.K. Maddocks, Paolo Paoli, Maria Letizia Taddei

Correspondence

erica.pranzini@unifi.it (E.P.), paolo.paoli@unifi.it (P.P.)

In brief

Pranzini et al. show that 5-FU resistance is supported by increased serine consumption and its mitochondrial compartmentalization to support purine biosynthesis and potentiate DNA damage repair to overcome drug toxicity. Interfering with serine accessibility and targeting mitochondrial serine metabolism overcome 5-FU resistance.

Pranzini et al., 2022, Cell Reports *40*, 111233
August 16, 2022
https://doi.org/10.1016/j.celrep.2022.111233

CellPress

Cell Reports

CellPress
OPEN ACCESS

Article

SHMT2-mediated mitochondrial serine metabolism drives 5-FU resistance by fueling nucleotide biosynthesis

Erica Pranzini,[1,*] Elisa Pardella,[1] Livio Muccillo,[2] Angela Leo,[1] Ilaria Nesi,[1] Alice Santi,[1] Matteo Parri,[1] Tong Zhang,[3,5] Alejandro Huerta Uribe,[3] Tiziano Lottini,[4] Lina Sabatino,[2] Anna Caselli,[1] Annarosa Arcangeli,[1] Giovanni Raugei,[1] Vittorio Colantuoni,[2] Paolo Cirri,[1] Paola Chiarugi,[1] Oliver D.K. Maddocks,[3] Paolo Paoli,[1,6,7,*] and Maria Letizia Taddei[4,6]

[1]Department of Experimental and Clinical Biomedical Sciences, University of Florence, Viale Morgagni 50, 50134 Florence, Italy
[2]Department of Sciences and Technologies, University of Sannio, Via Francesco de Sanctis, 82100 Benevento, Italy
[3]Institute of Cancer Sciences, Wolfson Wohl Cancer Research Centre, University of Glasgow, Switchback Road, Glasgow G61 1QH, UK
[4]Department of Experimental and Clinical Medicine, University of Florence, Viale Morgagni 50, 50134 Florence, Italy
[5]Novartis Institutes for BioMedical Research, Shanghai, China
[6]These authors equally contributed
[7]Lead contact
*Correspondence: erica.pranzini@unifi.it (E.P.), paolo.paoli@unifi.it (P.P.)
https://doi.org/10.1016/j.celrep.2022.111233

SUMMARY

5-Fluorouracil (5-FU) is a key component of chemotherapy for colorectal cancer (CRC). 5-FU efficacy is established by intracellular levels of folate cofactors and DNA damage repair strategies. However, drug resistance still represents a major challenge. Here, we report that alterations in serine metabolism affect 5-FU sensitivity in *in vitro* and *in vivo* CRC models. In particular, 5-FU-resistant CRC cells display a strong serine dependency achieved either by upregulating endogenous serine synthesis or increasing exogenous serine uptake. Importantly, regardless of the serine feeder strategy, serine hydroxymethyltransferase-2 (SHMT2)-driven compartmentalization of one-carbon metabolism inside the mitochondria represents a specific adaptation of resistant cells to support purine biosynthesis and potentiate DNA damage response. Interfering with serine availability or affecting its mitochondrial metabolism revert 5-FU resistance. These data disclose a relevant mechanism of mitochondrial serine use supporting 5-FU resistance in CRC and provide perspectives for therapeutic approaches.

INTRODUCTION

Despite constant progress in developing successful anticancer strategies (Leary et al., 2018), drug resistance still hinders therapeutic advance. The great metabolic plasticity of cancer cells contributes to the emergence of resistant clones (Desbats et al., 2020; Pranzini et al., 2021). Modulating tumor metabolism is, therefore, a promising strategy to manage therapy outcomes (Zecchini and Frezza, 2017) and recognizing metabolic modifications supporting drug resistance represents an essential step for developing effective approaches to prevent and target drug resistance.

5-Fluorouracil (5-FU) is a primary chemotherapy agent for the management of multiple solid malignancies, including advanced and metastatic colorectal cancer (CRC) (Vodenkova et al., 2020). 5-FU exerts its toxicity on cancer cells by interfering with nucleotide biosynthesis and nucleotide pool composition (Longley et al., 2003), primarily by inhibiting thymidylate synthase (TS) (Peters et al., 2002). In addition, 5-FU derivates are mis-incorporated into DNA and RNA with consequent genotoxic damages (Longley et al., 2003). Multiple factors, including drug metabolism and drug target expression alterations, contribute to 5-FU resistance (Zhang et al., 2008). Interestingly, 5-FU disrupts the flux toward one-carbon metabolism (OCM) (Ser et al., 2016), hinting that 5-FU-resistant cells may undergo specific reprogramming in this pathway. However, to date, little evidence has been provided to support its role in 5-FU resistance.

The OCM network integrates the folate and methionine cycles with serine and glycine metabolism supporting essential functions in cancer cells (Ducker and Rabinowitz, 2017). In particular, serine metabolism plays a crucial role in cancer biology by fostering biosynthetic pathways and fast proliferation (Yang and Vousden, 2016). Serine can be taken up from the extracellular milieu or synthesized through the *de novo* serine synthesis pathway (SSP), frequently overexpressed in cancers (Locasale et al., 2011; Pollari et al., 2011; Possemato et al., 2011). Both SSP inhibition (Pacold et al., 2016) and serine starvation (Maddocks et al., 2013, 2017) decrease cancer growth, especially when these two approaches are combined (Tajan et al., 2021).

Here we outline a pivotal role of serine metabolism in mediating 5-FU resistance in CRC. We identify the specific

compartmentalization of serine-derived carbons inside the mitochondria as a driving strategy in 5-FU resistance, supporting purine biosynthesis and DNA damage response.

RESULTS

Serine availability determines 5-FU sensitivity in CRC

To assess the involvement of serine metabolism in 5-FU sensitivity, we tested 10 CRC cell lines (HCT-116, HT29, HCT8, CACO-2, DLD1, LoVo, RKO, LS174T, COLO 205, and SW-1116) characterized by different oncogenic mutations and genomic stabilities (Ahmed et al., 2013). The expression of the first rate-limiting enzyme in the SSP, 3-phosphoglycerate dehydrogenase (PHGDH), is an heterogeneous factor influencing cancer cell proliferation (Locasale et al., 2011) and metastasis formation (Rossi et al., 2022). However, little evidence highlighted its role in anticancer drug response.

Interestingly, we found substantial differences among the analyzed cell lines at both PHGDH mRNA and protein levels (Figure S1A, Figures 1A and 1B), allowing the classification of high-PHGDH and low-PHGDH cells (Figure 1B). Interestingly, high-PHGDH cells (HCT-116, HCT8, LS174T, and SW-116) are characterized by a decreased 5-FU sensitivity compared with low-PHGDH cells (HT29, CACO-2, DLD1, LoVo, RKO, and COLO 205) (Figure 1C) showing a strong correlation between PHGDH levels and 5-FU response (Figure 1D). In addition, we did not find a similar correlation between protein levels of the other two SSP enzymes (phosphoserine aminotransferase 1 [PSAT-1] and phosphoserine phosphatase [PSPH]) and 5-FU response (Figure S1B). By incubating HCT-116 and HT29 cells (respectively representative of PHGDH-high/PSPH-low and PHGDH-low/PSPH-high cell lines) with uniformly labeled glucose ([U-^{13}C]-glucose]), we measured higher serine M+3 in HCT-116 than HT29 (Figure S1C), confirming the driving role of PHGDH in modulating SSP activity. By measuring serine content in the media conditioned by cancer cells, we found an extensive consumption of extracellular serine (Figure 1E), but not glycine (Figure S1D), by all the analyzed cell lines, particularly by the PHGDH-low cells CACO-2 and RKO. In accordance, by culturing CRC cell lines with [1-2^{14}C]-serine, we observed that PHGDH-low cells CACO-2 and RKO display greater exogenous serine uptake than PHGDH-high cells (Figure 1F).

To determine the contribution of serine availability to a 5-FU-adaptive response, we investigated the effect of serine and glycine (ser/gly) withdrawal on PHGDH-low cells under 5-FU treatment. Cells were let to proliferate in standard medium (+ser +gly) or medium lacking ser/gly in the presence or not of non-lethal doses of 5-FU. While the sole removal of ser/gly from the culture medium affects cell proliferation (Figures S1E–S1H), combining ser/gly starvation with 5-FU treatment further decreases the survival rate of all the analyzed PHGDH-low cell lines (Figures 1G–1I). Similarly, 5-FU treatment in the presence of a minimal effective concentration of NCT-503 (Figures S1I–S1K), a specific PHGDH inhibitor (Pacold et al., 2016), significantly affects PHGDH-high cells survival (Figures 1J–1L).

Together, these results highlight that serine availability supports 5-FU response in CRC cells and reveal that displaying high-PHGDH could represent an intrinsic advantage under 5-FU treatment.

Decreasing serine availability increases 5-FU anticancer effects *in vivo*

To investigate the *in vivo* antitumor efficacy of targeting serine metabolism in combination with 5-FU based-therapies, we used a syngeneic mouse model of CRC. Balb/c mice were subcutaneously injected with CT26 cells and maintained on a normal diet until measurable tumors had formed. Tumor-bearing mice were then placed on a control diet or a diet lacking ser/gly (–S –G diet). Three days after diet change, mice were treated either with vehicle or 5-FU (40 mg/kg) with a cyclic regimen composed of three subsequent daily injections followed by two recovery days (Figure 2A). Quantifying circulating metabolite levels at the experiment's endpoint indicated that dietary deprivation of ser/gly decreases plasma levels of these amino acids, in accordance with previous reports (Maddocks et al., 2017) (Figures S1M and S1O). Unlike what we observed *in vitro* by depriving CT26 of ser/gly (Figure S1L), the sole dietary intervention does not impact tumor growth (Figures 2B and 2C), suggesting that *in vivo* CT26 cells can obtain serine from other sources than the diet. Coherently, ser/gly deprivation does not impact their intra-tumor abundance (Figures 1N and 1P). However, the combination of a –S –G diet with 5-FU treatment potentiates the drug's efficacy in inhibiting tumor growth (Figure 2B), significantly decreasing the total tumor mass at the endpoint of the experiment (Figure 2C). These results indicate that serine availability affects 5-FU antitumor efficacy *in vivo*. Interestingly, 5-FU administration alone decreases ser/gly (Figures 2D and 2E) circulating levels and increases intra-tumor serine (but not glycine) levels. Besides, removing ser/gly from the diet rescues this intra-tumor serine accumulation, suggesting that it is specifically necessary for 5-FU response in cancer cells (Figures 2F and 2G).

To assess whether inhibiting PHGDH may potentiate 5-FU efficacy, we tested the combination of NCT-503 with 5-FU *in vivo*. Balb/c mice bearing CT26-derived tumors were intraperitoneally injected daily with vehicle or NCT-503 (40 mg/kg) together with a cyclic 5-FU regimen (Figure 2A). According to *in vitro* data (Figure 2H), this approach was more efficacious in decreasing tumor growth than the 5-FU treatment alone (Figure 2I). Together, these data demonstrate that interfering with serine availability by limiting its circulating levels or inhibiting SSP activity is an effective strategy to potentiate 5-FU antitumor effects *in vivo*.

Selected 5-FU-resistant CRC cells are strictly dependent on serine availability for survival and proliferation

Exposure to 5-FU may induce the selection of resistant clones displaying molecular and metabolic features to survive the treatment. To investigate whether the acquisition of 5-FU resistance by CRC cells relies on serine availability, we developed two *in vitro* models of 5-FU resistance by treating HCT-116 and HT29 cell lines with increasing concentrations of 5-FU up to 20 μM (referred to as "HCT-116R″ and "HT29R″, respectively) (Denise et al., 2015). HCT-116 and HT29 cell lines are two CRC cell lines with different mutation statuses: HCT-116 displays mutations in PI3KCA and K-RAS genes conferring constitutive

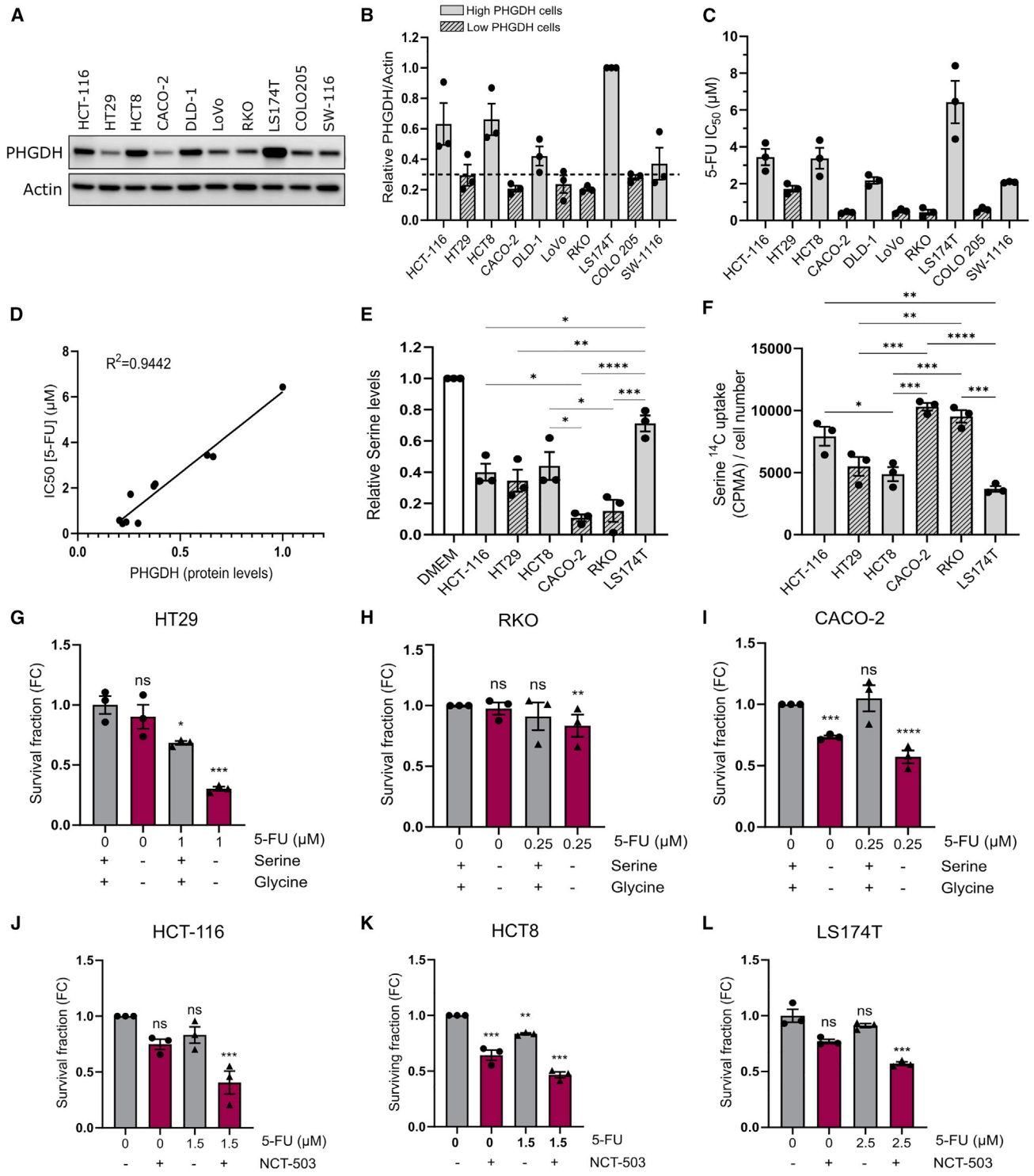

Figure 1. Endogenous/exogenous serine driving 5-FU response in CRC

(A and B) (A) PHGDH protein levels in CRC cell lines. The image is representative of three independent experiments. (B) Quantification of PHGDH protein levels normalized on Actin. Data are reported as fold change using LS174T cells as reference (n = 3).

(C) CRC cell lines viability under 5-FU treatment. Data are reported as half maximal inhibitory concentration (IC_{50}) values after 48 h of treatment. Cell lines were classified as high-PHGDH or low-PHGDH cells according to relative PHGDH/actin values reported in Figure 1B (cut-off value 0.3, arbitrary units). (B, C) Statistics in Table S1 (n = 3).

(D) Pearson correlation between PHGDH expression and 5-FU survival rate on CRC cell lines.

(legend continued on next page)

activation of PI3K/AKT and K-RAS pathways (Wang et al., 2007), while HT29 displays a DNA binding-defective p53 mutant form (R273H p53 mutant) (Davidson et al., 2012). The resistant clones display sustained cell viability under drug treatment (Figure S2A), persistent clonogenic ability after drug exposure (Figures S2B–S2D), and increased TS levels (Figure S2E).

Analyzing the expression of SSP-related enzymes, we found increased PSAT-1 and PSPH levels in HCT-116R and PSAT-1 levels in HT29R compared with parental cells (Figures 3A–3C). By contrast, PHGDH mRNA and protein levels are enhanced in HCT-116R but not in HT29R (Figures 3D and 3E). Although the expression of PHGDH, PSAT-1, and PHPH share common mechanisms of regulation, specific regulatory mechanisms have been identified for PHGDH (Dalton et al., 2019; DeNicola et al., 2015; Locasale et al., 2011; Ou et al., 2015; Possemato et al., 2011; Riscal et al., 2016). Tumors harboring different p53 mutations differentially respond to serine-starved conditions by inducing SSP enzymes (Humpton et al., 2018; Maddocks et al., 2013) in a mechanism mediated by MDM2 recruitment to chromatin and ATF/NRF2-dependent transcriptional program activation (DeNicola et al., 2015; Riscal et al., 2016). Notably, HCT-116 cells are p53 wild type, while HT29 cells harbor R273H p53 mutation, thus failing p21 and MDM2 induction (and NRF2 nuclear localization) (Figure S2F). Consequently, HT29 cells express low PHGDH protein levels (Figure 3F). In line, silencing p53 in HCT-116 cells results in decreased PHGDH levels (Figure 3F) and increased susceptibility to ser/gly deprivation (Figure S2G), as well as decreased tolerance to 5-FU treatment (Figure S2G). Moreover, silencing PHGDH (Figure S3A) enhances 5-FU sensitivity in HCT-116 (Figure S3B) and HCT-116R cells (Figure 3G), but does not affect 5-FU response in HT29 and HT29R cells (Figures S3C and S3D). NCT-503 treatment (minimal effective concentration) (Figure S3E) rescues 5-FU sensitivity in HCT-116R cells (Figure 3H), while HT29R cells are not affected by NCT-503 treatment provided either as a single agent or in combination with 5-FU (Figure S3F). These results are in line with our data indicating that HT29 cells, displaying low levels of PHGDH compared with other analyzed CRC cell lines, mostly rely on exogenous serine. Coherently, [U-^{13}C]-glucose labeling revealed no SSP activity in HT29R cells (Figure S1C). These results demonstrate that PHGDH expression alone is not a driving determinant of 5-FU resistance but could represent an adaptive response under specific mutational contexts.

Besides, resistant clones might rely differently on exogenous serine as a 5-FU adaptive response. By measuring [1-2^{14}C]-serine cellular incorporation, we found higher exogenous serine uptake in HT29R cells than their parental counterpart, while no significant differences were observed in the two HCT-116 clones (Figure 3I). Serine can be transported into the cell through different transporters, including the sodium-dependent transporters ASC (ASCT1/SLC1A4 and ASCT2/SLC1A5) and the sodium- and chloride-dependent neutral and basic amino acid transporter SLC6A14 (Bröer and Bröer, 2017). We found a significant increase in SLC1A4 and SLC6A14 transporters in HT29R with respect to parental cells (Figures 3J and 3K). Furthermore, under ser/gly starvation, HT29R cells undergo a stronger proliferation arrest than their parental counterpart (Figures S2H and S2I), while HCT-116R cells are not affected by ser/gly withdrawal (Figure S2K) and are more tolerant to the deprived conditions than the corresponding parental cells (Figure S2J). In accordance, depleting HT29R cells of exogenous ser/gly has a more prominent effect in decreasing cell survival than 5-FU treatment alone (Figure 3L), and potentiates the 5-FU antiproliferative effects (Figure S3G). Interestingly, acute treatment with 5-FU induces an increase in exogenous serine uptake in both resistant cell lines (Figures 2L and 2M).

To confirm these observations *in vivo*, we carried out a xenograft experiment with HT29R cells, feeding animals with a control diet or a –S –G diet after tumor formation, and we evaluated the efficacy of this dietary approach to potentiate 5-FU activity against resistant tumors (cyclic regimen as described in Figure 2A). Confirming the maintenance of the resistant phenotype, 5-FU treatment does not affect HT29R-derived tumor growth (Figures 3M, 3N; Figures S3H–S3J). As previously observed (Figures 2B and 2C), the sole dietary approach does not significantly impact final tumor size. However, combining the –S –G diet with a 5-FU regimen overcomes therapy resistance and affects tumor size after two weeks of treatment (Figures 3M and 3N; Figures S3H–S3J). Interestingly, 5-FU treatment decreases plasma serine levels (Figure 3O), potentiating the effect of ser/gly dietary deprivation (Figures SK and SL).

Together, these data show that 5-FU acquired resistance confers a specific dependency on serine availability, which is achieved by resistant clones either by enhancing SSP activity or increasing exogenous serine uptake depending on the genetic background and the basal PHGDH expression.

Untargeted metabolomic analysis of 5-FU-resistant CRC cells reveals an adaptive alteration in nucleotide metabolism

Untargeted metabolomic analysis allowed to investigate the metabolic adaptations underpinning 5-FU resistance. By comparing the metabolic profile of HCT-116 and HCT-116R cells, we identified a set of metabolites significantly altered between two clones (Figure 4A), including key intermediates of nucleotide metabolism. Coherently, ingenuity analysis of the

(E) Serine content in culture media conditioned by CRC cells for 48 h. Metabolites from serum-free CRC cells conditioned media normalized to corresponding cell number using DMEM as a reference (n = 3).

(F) Exogenous serine uptake in CRC cell lines. [1-2^{14}C]-serine incorporated by CRC cells expressed in counts per minute (CPM) and normalized on cell number. (E, F) One-way ANOVA with Tukey's *post hoc* test (n = 3).

(G–I) Survival fraction of HT29, CACO-2, and RKO cells treated or not with 5-FU in combination with serine/glycine starvation for 48 h. Non-treated cells were used as a reference.

(J–L) Survival fraction of HCT-116, HCT8, and LS174T cells treated or not with 5-FU and NCT-503 Cells were treated with 10 μM NCT-503 for 48 h. Non-treated cells were used as a reference. (G-L) One-way ANOVA with Dunnett's *post hoc* test (n = 3). Each dot represents a single experiment. Data are represented as mean ± standard error of the mean of at least three independent biological replicates. ns, not significant. *p < 0.05, **p < 0.01, ***p < 0.001.

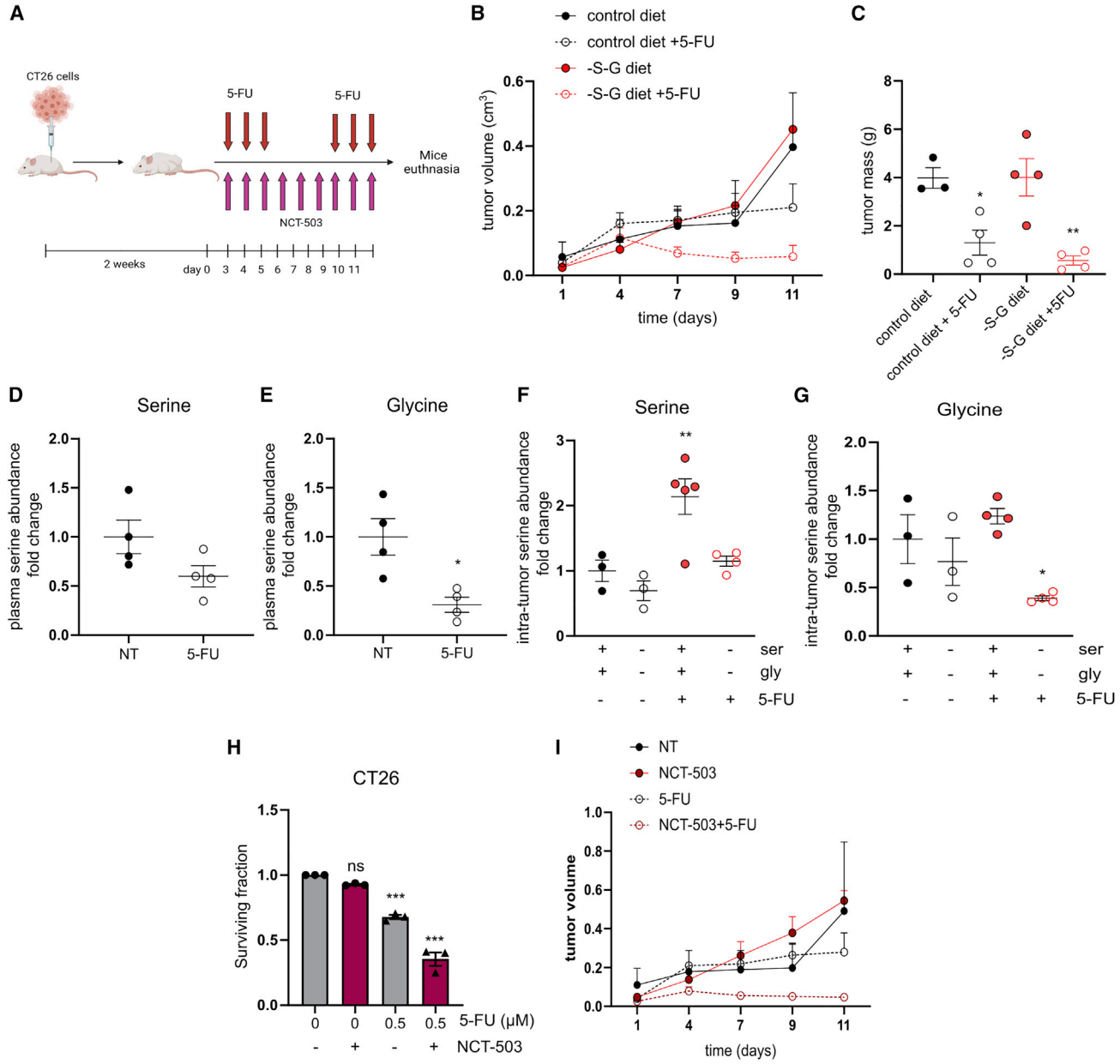

Figure 2. Serine deprivation increases 5-FU efficacy *in vivo*

(A) Workflow for the *in vivo* assessment of 5-FU sensitivity under serine-deprived conditions.

(B and C) Tumor growth curve and (C) total tumor mass in Balb/c mice subjected to control or –S –G diet and treated with/without 40 mg/kg 5-FU as described in (A). One-way ANOVA with Sidak *post hoc* test ($n \geq 3$).

(D and E) Relative plasma serine (D) and glycine (E) levels in mice fed with control diet and treated with/without 5-FU. Each dot represents a plasma sample from a single mouse. Student's t test ($n \geq 3$).

(F and G) Intra-tumor serine (F) and glycine (G) levels in mice fed with control diet and treated with/without 5-FU. Each dot represents a tissue sample from a single mouse. Student's t test ($n \geq 3$).

(H) Survival fraction of CT26 cells treated or not with 5-FU in combination with NCT-503 10 μM for 48 h. Non-treated cells were used as a reference. One-way ANOVA with Dunnett's *post hoc* test (n = 3). Each dot represents a single experiment.

(I) Tumor growth curve in mice treated or not with 5-FU with or without NCT-503 as described in (A). One-way ANOVA with Sidak *post hoc* test ($n \geq 3$). Data are represented as mean ± standard error of the mean of n mice per group. ns, not significant. *$p < 0.05$, **$p < 0.01$, ***$p < 0.001$.

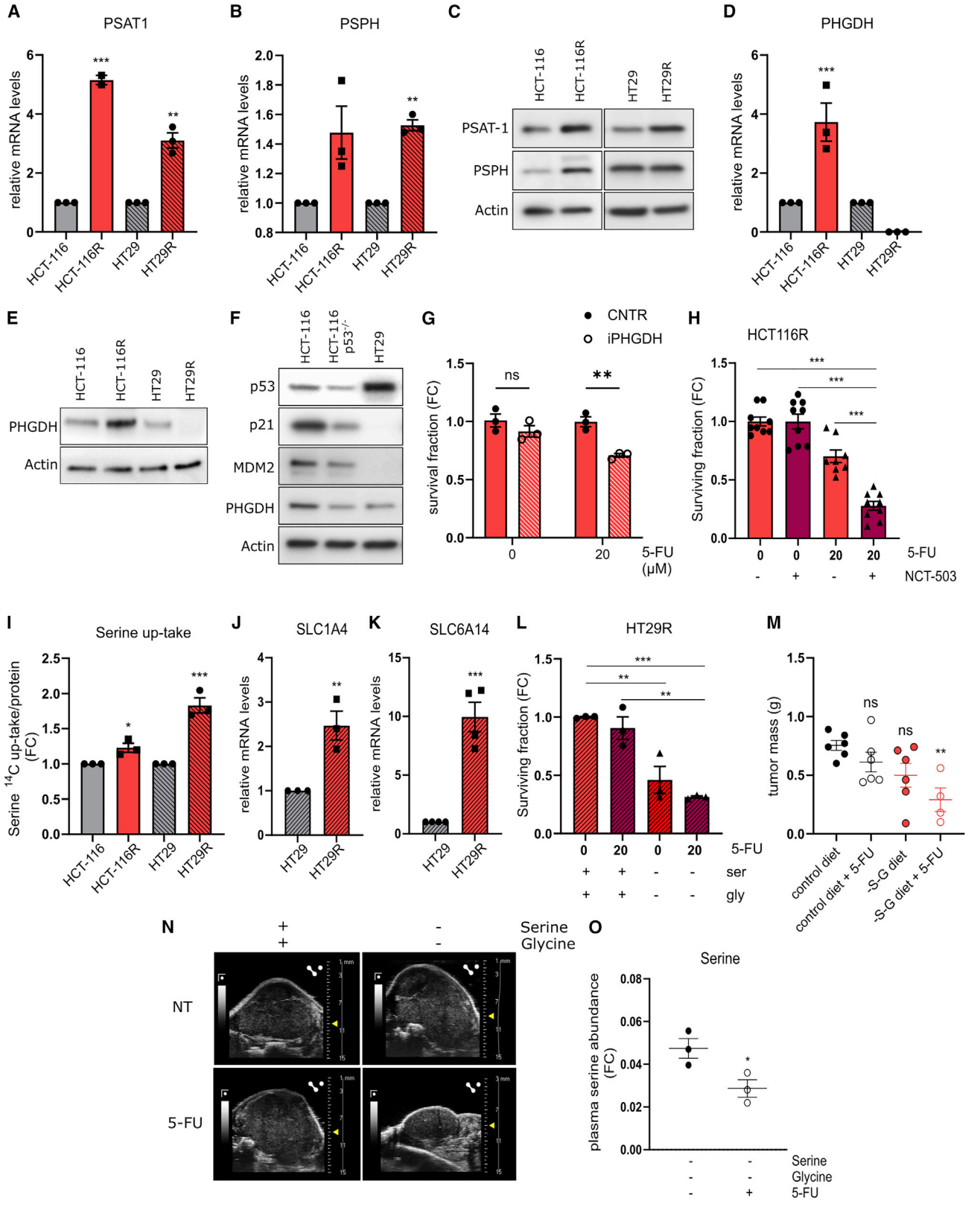

(legend on next page)

leading pathways in which the resulting metabolites participate indicated that the acquisition of 5-FU resistance has the most significant impact on alanine, aspartate, glutamine-glutamate, and nucleotide metabolism (Figure 4B).

Comparing the abundance of nucleotide-related metabolites in resistant versus parental cells revealed a strong accumulation of all the intermediates of the pyrimidine biosynthetic pathway (pyr-P) (Figure 4C) and a significant increase of the main purine biosynthetic pathway (pur-P) intermediates, namely FGAR, FAICAR, AICAR, and SAICAR (Figure 4D). No significant differences were detected in the total levels of the purine precursor IMP (Figure S4A) and the final pur-P products AMP (Figure S4B) and guanosine monophosphate (GMP) (Figure S4C), but a substantial increase in uridine 5'-monophosphate (UMP) (Figure S4D) and 2'-deoxyuridine 5'-monophosphate (Figure S4E).

To better understand the activity of the pyr-P and the pur-P biosynthetic pathways, we performed a stable isotope tracing analysis by culturing cells in a medium supplemented with [U-^{13}C]-glucose for 30 min, 1 h, and 3 h, and quantifying glucose-derived carbons incorporation into the final products of the two pathways. Glucose mainly contributes carbons to UMP and AMP/GMP through the pentose phosphate pathway (PPP) for a total of five carbons. A substantial decrease in glucose 6-phosphate M+5 and an increase in ribose 5-phosphate M+5 in HCT-116R compared with HCT-116 cells (Figures S4F and S4G) indicated an increase in the PPP activity (Figure S4H). No significant difference was found in the relative abundance of the M+5 isotopomers of UMP (Figure 4E), but we observed a more prominent increase in AMP and GMP M+5 isotopomers relative abundance over time in HCT-116R than in parental cells (Figures 4F and 4G). The accumulation of the pyr-P intermediate and the observed isotope labeling pattern suggest an inhibition of the downstream enzymes with a subsequent slowdown of the overall flux through the pathway. Conversely, the slight accumulation of the pur-P intermediates, alongside the rise in M+5 labeling after [U-^{13}C]-glucose incubation, demonstrate an increase in the flux toward pur-P in resistant cells.

Serine supports purine biosynthesis and DNA damage response in 5-FU-resistant CRC cells

Serine can be used for different biosynthetic functions, among which the synthesis of glutathione (GSH), S-adenosylmethionine (SAM) and purines starting from IMP are essential in tumor progression (Figure 5A) (Newman and Maddocks, 2017). To determine the fate of serine-derived carbons in 5-FU-resistant clones, we cultured cells in a medium supplemented with uniformly labeled serine ([U-^{13}C]-serine) and measured serine incorporation into its main derivatives. Interestingly, this analysis revealed that serine mainly supports purine biosynthesis in resistant cells, as demonstrated by increased M+2, M+3, and M+4 IMP after [U-^{13}C]-serine incubation (Figure 5B). A similar labeling pattern was observed in AMP (Figure 5C; Figure S4I) and SAM (Figure 5C), reflecting the fact that SAM is built from the cellular AMP pool (Maddocks et al., 2016). Conversely, no significant differences were found in the contribution of serine to GSH (Figure 5E; Figure S4J).

Decreased susceptibility to genotoxic agents is frequently associated with altered nucleotide metabolism supporting DNA damage repair (Pranzini et al., 2021). The quantification of histone H2AX phosphorylation (γH2AX), a known marker of DNA double-strand break (Mah et al., 2010), proves that resistant clones from both cell lines display enhanced ability to prevent DNA damage accumulation following 5-FU exposure (Figure 5F). Analyses of γH2AX levels after 5-FU treatment upon serine depletion confirmed that serine is required to support DNA damage response in resistant clones. NCT-503 treatment in HCT-116R cells (Figure 5G) or ser/gly deprivation in HT29R cells (Figure 5H) rescue γH2AX accumulation under 5-FU exposure. To confirm the hypothesis that serine supports 5-FU resistance by fueling purine (but not pyrimidine) biosynthesis, we tested the ability of the exogenous nucleotide precursors hypoxanthine

Figure 3. Selected 5-FU-resistant CRC cells display enhanced serine dependency

(A, B, and D) mRNA levels of SSP enzymes in selected 5-FU-resistant CRC cell lines. PSAT-1 (A), PSPH (B), and PHGDH (D) mRNA expression levels analyzed by quantitative RT-PCR using parental cells as comparator. Student's t test (n = 3).

(C and E) SSP enzymes protein levels in selected 5-FU-resistant and sensitive CRC cell lines. Total protein lysates from HCT-116, HCT-116R, HT29, and HT29R cells were extracted and analyzed for PSAT-1, PSPH (C) and PHGDH (E).

(F) p53/MDM2-mediated modulation of PHGDH. Total protein lysates from HCT-116, p53$^{-/-}$ HCT-116, and HT29 cells were analyzed for p53, p21, MDM2, and PHGDH protein levels. (C, E–F) Actin was used as loading control. The images are representative of three independent experiments.

(G) Survival fraction of PHGDH-silenced HCT-116R cells under 5-FU treatment. Cells were transfected with PHGDH-targeting siRNA or negative control and treated with 5-FU for 48 h. Non-transfected/treated cells were used as comparator. two-way ANOVA with Sidak's *post hoc* test (n = 3).

(H) Survival fraction of HCT-116R cells treated or not with 5-FU in combination with NCT-503 (10 μM for 48 h). Non-treated cells were used as a reference. One-way ANOVA with Tukey's *post hoc* test ($n \geq 8$).

(I) Exogenous serine uptake in CRC 5-FU resistant cells. [1-2^{14}C]-serine incorporation normalized on cell number and expressed using respective parental cells as a comparator. Student's t test (n = 3).

(J and K) mRNA levels of serine transporters in HT29R cells. SLC1A4 (J) and SLC6A14 (K) mRNA expression levels in HT29 and HT29R cells by quantitative RT-PCR using parental cells as comparator. Student's t test (n = 3).

(L) Survival fraction of HT29R cells treated or not with 5-FU in presence or absence of ser/gly for 48 h. Non-treated cells were used as a reference. One-way ANOVA with Tukey's *post hoc* test (n = 3).

(M) Total tumor mass in HT29R cells-derived tumor-bearing Athymic Nude mice subjected to control or –S –G diet and treated with or without 5-FU as described in (Figure 2A). One-way ANOVA with Sidak *post hoc* test (n = 6).

(N) Representative high-resolution ultrasound images of subcutaneous tumors (n = 6).

(O) Relative plasma serine levels in mice fed with control diet and treated with/without 5-FU. Each dot represents a plasma sample derived from a single mouse. Student's t test- (A-L) (n = 3). Each dot represents a single experiment. Data are represented as mean ± standard error of the mean of at least three independent experiments. ns, not significant. *p < 0.05, **p < 0.01, ***p < 0.001.

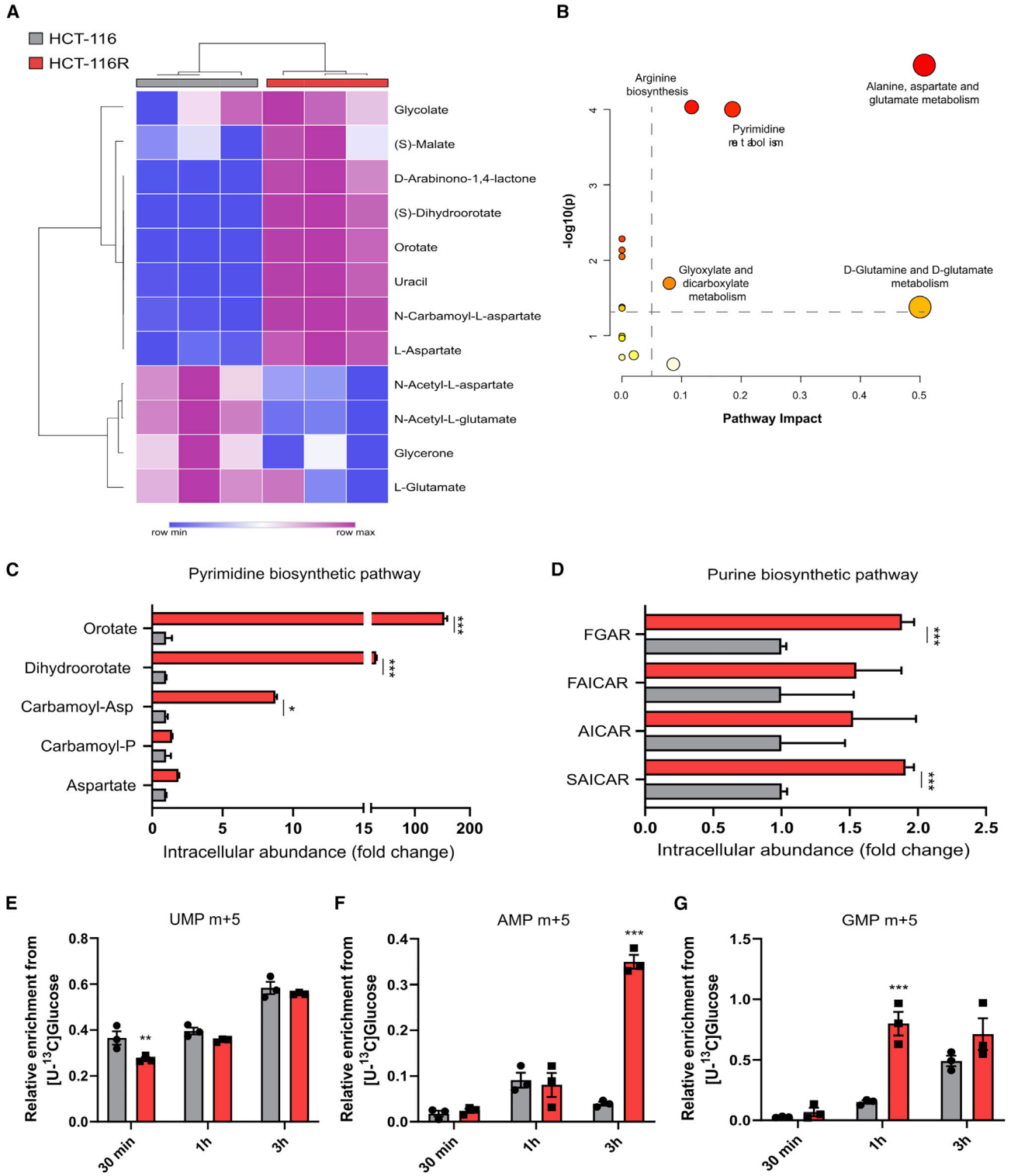

Figure 4. Selected 5-FU resistant cells show altered nucleotide metabolism profile

(A) Heatmap shows metabolite abundance in HCT-116R cells compared to HCT-116 cells. Two-way ANOVA with false discovery rate correction (n = 3).

(B) Bubble plot summarizing metabolites pathway analysis as in (A). The vertical dashed line indicates an arbitrary pathway enrichment threshold (>5%); the horizontal dashed line shows a statistical significance threshold ($p < 0.05$).

(C) Relative levels of pyr-P intermediates.

(legend continued on next page)

and thymidine to overcome 5-FU-induced DNA damage accumulation under serine deprivation. Hypoxanthine (but not thymidine) supplementation rescues 5-FU toxic effects (Figures 5I and 5J) and prevents DNA damage accumulation under serine-limiting conditions (Figures 5K and 5L) in resistant cells. Notably, specific targeting of the pur-P by treating with the glycinamide ribonucleotide formyltransferase inhibitor lometrexol decreases cell survival and potentiates the toxic effect of 5-FU on resistant cells (Figures 5M and 5N). Similarly, the antimetabolite drug pemetrexed selectively sensitizes resistant cells to 5-FU treatment (Figures S5A and S5B), indicating that targeting nucleotide biosynthesis at different levels is an effective strategy to counteract 5-FU resistance. In summary, increased serine dependency in 5-FU-resistant cells supports DNA damage repair under genotoxic drug pressure by fueling purine biosynthesis. Targeting serine availability enhances 5-FU-induced DNA damage in resistant cells, thereby increasing drug toxicity.

Resistance to 5-FU is supported by mitochondrial compartmentalization of OCM

The OCM is compartmentalized between the cytoplasm and the mitochondria (Ducker and Rabinowitz, 2017) thanks to the differential localization of the two isoforms of the serine hydroxymethyl-transferase (SHMT): the cytosolic SHMT1 and the mitochondrial SHMT2 (Ducker et al., 2016). Serine-derived carbons are incorporated into purines via glycine and 10-formyl-THF generated by SHMT2, while SHMT1 mainly provides 5,10-methylenetetrahydrofolate to support dTMP biosynthesis (Ducker et al., 2017; Fan et al., 2019). Interestingly, we found a decrease in SHMT1 and an increase in SHMT2 mRNA (Figures 6A and 6B), resulting in increased SHMT2/SHMT1 ratio at protein levels in 5-FU-resistant clones in both cell lines (Figures 6C and 6D). Remarkably, a higher SHMT2/SHMT1 ratio correlates with lower 5-FU toxicity in different CRC cell lines (Figures 6E; Figure 1C). Confirming a shift toward the mitochondrial branch of OCM, resistant cells display increased mRNA and protein levels of the primary mitochondrial serine transporter sideroflexin 1 (SFXN1) (Kory et al., 2018) (Figures 6F and 6H) and the mitochondrial glycine decarboxylase (GLDC) (Zhang et al., 2012) (Figures 6G and 6H). Coherently, HCT-116R cells display enhanced serine-derived CO_2 production (Figure S5C), confirming increased GLDC system activity.

By incubating cells with [U-^{13}C]-serine and subsequently treating them with digitonin to selectively permeabilize cytosolic membranes, we analyzed metabolites from both mitochondrial and cytoplasmic compartments by GC-MS (Nonnenmacher et al., 2019). [$^{13}C_3$]-serine generates [$^{13}C_2$]-glycine and [^{13}C]-methylene-THF inside mitochondria through the action of SHMT2. [^{13}C]-methylene-THF recombines with unlabeled glycine by the activity of SHMT1 in the cytosol to generate [$^{13}C_1$]-serine (Figure 6I). The amount of cytosolic [$^{13}C_1$]-serine thus reads out mitochondrial-derived methylene-THF production. The higher levels of [$^{13}C_1$]-serine in the cytosolic fraction of resistant cells confirm the hypothesized compartmentalization (Figure 6J). In addition, mitochondrial serine, mostly labeled on three carbons, indicates that exogenous serine is rapidly incorporated into the mitochondria to be metabolized by SHMT2 (Figure 6J).

Mitochondrial serine catabolism by SHMT2 fuels mitochondrial oxidative phosphorylation (OXPHOS). Indeed, serine catabolism by SHMT2 might regulate the OXPHOS gene expression by influencing mtDNA replication (Anderson et al., 2011) through the modulation of cellular nucleotide homeostasis (Bao et al., 2016), and driving the biosynthesis of the mitochondria-encoded OXPHOS proteins (Lucas et al., 2018; Minton et al., 2018; Morscher et al., 2018; Tani et al., 2018). Coherently, we found an enhanced oxygen consumption rate (OCR) in resistant versus parental cells (Figures 5D–5F; Figures S5G–S5I). Concordantly, confocal microscopy imaging showed a well-organized (Figure 6R) and more abundant (Figures S5J and S5K) mitochondria in resistant cells with respect to sensitive ones. In keeping, concomitant deprivation of exogenous ser/gly decreases basal (Figures 6K and 6L), maximal (Figures 6M and 6N), and ATP production-linked (Figures 6O and 6P) OCR in HCT-116R and HT29R, while it does not affect OCR parameters in parental cells. Notably, the sole serine supplementation rescues oxygen consumption in HCT-116R and HT29R cells (Figures 6K–6P), indicating that serine availability is necessary for mitochondrial functionality in 5-FU-resistant cells. Recently, it has been demonstrated that the oxidation of the serine-derived one-carbon units contributes to the redox potential to drive ATP synthesis via OXPHOS (Tedeschi et al., 2013; Vazquez et al., 2011). Coherently, resistant cells from both cell lines display higher intracellular levels of ATP (Figure 6Q). Silencing SHMT2 decreases ATP content in HCT-116R and HT29R cells (Figure 6S) and impairs mitochondria abundance (Figure 6T; Figures S5L and S5M). Together, these results indicate that the mitochondrial compartmentalization of ser/gly metabolism correlates with 5-FU resistance in CRC, supporting increased mitochondrial respiration.

Interfering with cytosolic and mitochondrial serine metabolism balance is effective in modulating 5-FU susceptibility in CRC

To investigate the impact of modulating SHMT1/2 balance in affecting 5-FU response, we tested the viability of SHMT1-deleted HCT-116 cells (HCT-116ΔSHMT1) (Ducker et al., 2017) (Figure S5N) after 5-FU exposure. Interestingly, HCT-116-ΔSHMT1 cells are less sensitive to the drug's toxic effect (Figure 7A) than parental cells, confirming that lower levels of SHMT1 facilitate the acquisition of 5-FU resistance. Moreover, SHMT1 deletion confers a more aggressive phenotype to HCT-116 cells, as indicated by the increased colony-forming ability after 5-FU treatment (Figure 7B). Otherwise, inhibiting SHMT2 in

(D) Relative levels of pur-P intermediates. Fold change metabolites content calculated using HCT-116 cells as reference. Student's t test (n = 3).
(E) UMP M+5 labeling enrichment after 24 h incubation with [U-^{13}C]-glucose.
(F) AMP M+5 labeling enrichment after 24 h incubation with [U-^{13}C]-glucose.
(G) GMP M+5 labeling enrichment after 24 h incubation with [U-^{13}C]-glucose. Cells were incubated in a medium containing [U-^{13}C]-glucose for 24 h before assessing intracellular metabolites labeling enrichment. two-way ANOVA with Sidak's *post hoc* test (n = 3). (A–G) Each dot represents a single experiment. Data are represented as mean ± standard error of the mean of at least three independent experiments. ns, not significant. *p < 0.05, **p < 0.01, ***p < 0.001.

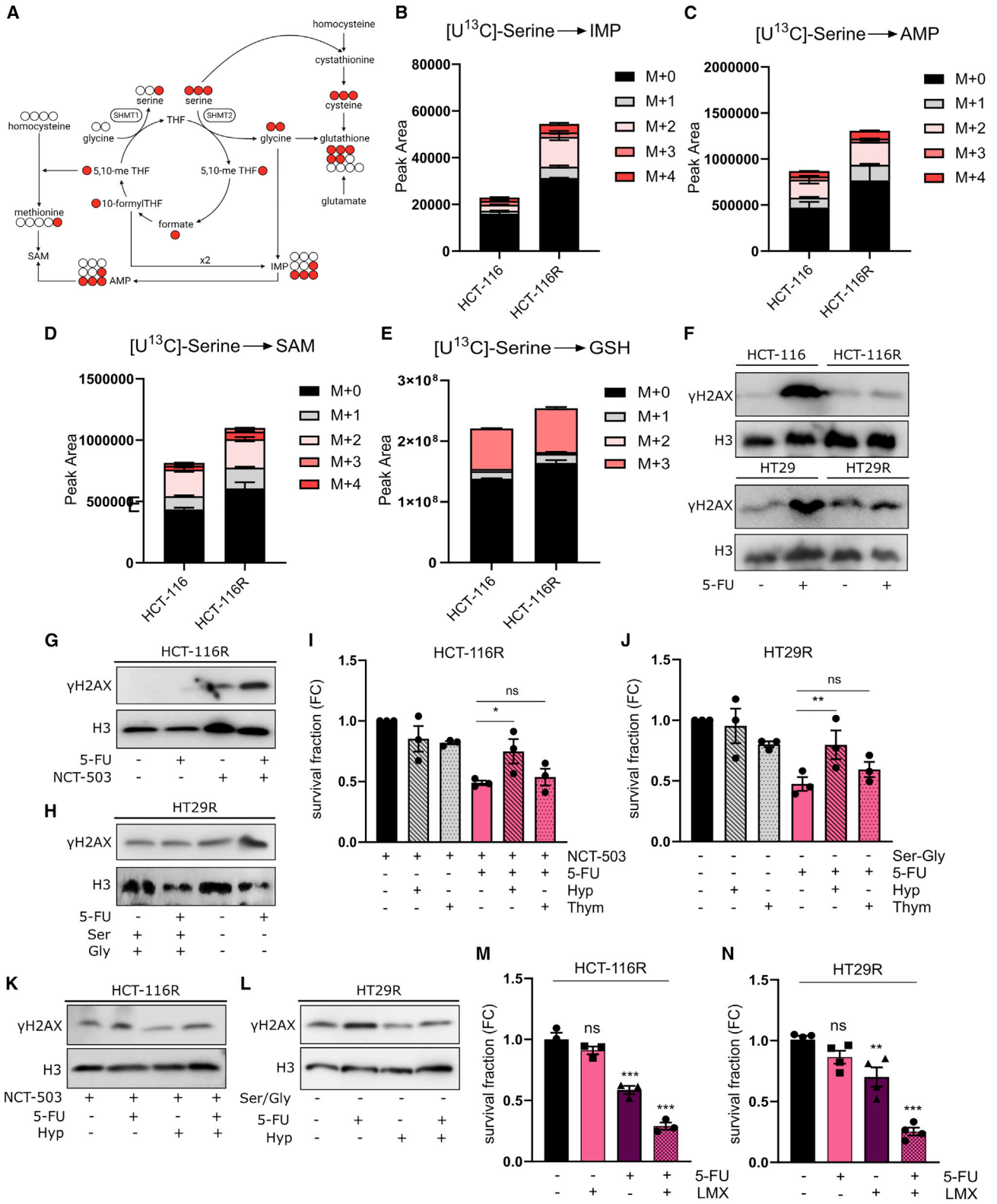

(legend on next page)

resistant cells could be an effective strategy to recapitulate 5-FU resistance. To evaluate the effect of targeting SHMT2 in resistant cells, we silenced SHMT2 in HCT-116R cells and assessed the impact on 5-FU response. Interestingly, SHMT2-silenced HCT-116R cells increase SHMT1 mRNA levels, while HCT-116 cells do not (Figure 7C). Increasing SHMT1 expression under SHMT2 deletion is a compensatory mechanism that represents a liability in 5-FU response. In accordance, SHMT2 silencing results in decreased cellular proliferation in HCT-116R (Figure 7D), while it does not affect HCT-116 cells growth Figure 7E). Moreover, SHMT2 silencing increases 5-FU toxicity in HCT-116R cells (Figure 7F), indicating that SHMT2 functionality is necessary to support 5-FU tolerance in resistant cells.

Analysis of the TCGA-COADREAD dataset confirms the nucleotides metabolism dependency of 5-FU non-responder patients

The clinical relevance of these results was validated by enquiring a retrospective CRC cancer patients' cohort selected from the TCGA-COADREAD dataset for their response to 5-FU-based therapies. Of 630 patients included in the cohort, we selected 338 based on their responsiveness to 5-FU administration (64 non-responders [NR] and 274 responders [R]). We found a statistically significant difference in the overall survival between R and NR patients, with the former displaying a better outcome (Figure S6A). We then surveyed differential expressed genes (DEGs) filtering for those coding for metabolic enzymes and proteins (Calvo et al., 2016; Corcoran et al., 2017; Pagliarini et al., 2008) to recognize the enriched pathways. Of note, drug resistance is strongly correlated with pathways enriched in tyrosine metabolism (Poliaková et al., 2018), while drugs sensitivity with those enriched amino acids and lipid metabolism (Park et al., 2005) (Figure S6B). These results are obtained by analyzing whole tumor tissues representing an average of the transcriptome of different cell types and thus lacking the resolution power to identify specific signatures of each cell type at the basis of CRC heterogeneity.

For a deeper analysis, we classified the patients into four subgroups according to the consensus molecular subtypes (CMS1-4) criteria (Guinney et al., 2015). We then examined DEGs and the related metabolic pathways between R and NR patients for each subtype. Among the several pathways recognized, purine metabolism was significantly upregulated in NR patients belonging to the CMS3 and CMS1 groups (Figure 7G), while pathways related to small molecule and amino acids biosynthetic processes, as well as small molecules catabolic processes, were enriched in R patients of the same subgroups (Figure 7G). The pathways enriched in CMS2 and CMS4 subgroups were only marginally affected (Figure 7G; Figure S6C).

Notably, the CMS1 population is characterized by a poor survival rate after relapse (Guinney et al., 2015). For this reason, we focused on the CMS1 population to investigate metabolic enzymes/proteins specifically altered in NR patients. Interestingly, we found adenylate cyclase 3, RNA polymerase III subunit A, and RNA polymerase I subunit A significantly upregulated in NR patients. At the same time, nucleoside diphosphate kinase 3, aldehyde dehydrogenase 2, and SHMT1 resulted to be significantly upregulated in R patients (Figure 7H). The upregulation of SHMT1 in the R cohort (Figure 7I) is in accordance with our *in vitro* data indicating that high levels of this isoform correlate with treatment efficacy in patients undergoing 5-FU-based therapies.

Together, these data strengthen the importance of metabolic adaptations promoting purine biosynthesis in reducing the efficacy of 5-FU-based therapies in patients with CRC. Interestingly, in the subgroup of patients displaying a worst prognosis after relapse, high SHMT1 expression provides an advantage under 5-FU-based therapies, resulting in a better response.

DISCUSSION

Cancer cells are highly dependent on serine metabolism, as it supports proliferative and pro-survival processes (Labuschagne et al., 2014; Yang and Vousden, 2016). Several studies reported the therapeutic advantage of targeting serine metabolism to

Figure 5. Serine metabolism supports purine biosynthesis and DNA damage repair in 5-FU-resistant cells

(A) Schematic representation of the serine-derived carbons fate into GSH, purines, and methionine synthesis.

(B–E) Incorporation of [U-^{13}C]-serine carbons in IMP (B), AMP (C), SAM (D), and GSH (E). HCT-116 and HCT-116R cells were incubated in a medium containing [U-^{13}C]-serine for 8 h before assessing intracellular metabolite labeling enrichment (n = 3).

(F) H2AX phosphorylation (γH2AX) levels in selected 5-FU-resistant and sensitive CRC cell lines. Proteins from nuclear compartments were analyzed by western blotting.

(G) Effects of 5-FU and NCT-503 co-treatment on H2AX phosphorylation levels in HCT-116R cells. Cells were grown either in the presence or not of 20 μM 5-FU and treated with 5 μM NCT-503 or vehicle for 48 h before analyzing proteins from nuclear compartments by western blotting.

(H) Effects of 5-FU treatment on γH2AX levels in HT29R cells under serine starvation. Cells were grown in a medium containing or lacking ser/gly and treated or not with 20 μM 5-FU for 48 h before analyzing the proteins from nuclear compartments by western blotting. (F–H) H3 was used as loading control. Each image is representative of at least three independent experiments.

(I-J) Providing purine and pyrimidine metabolites rescues 5-FU toxicity of resistant cells under serine-deprived conditions. Surviving fraction of HCT-116R (I) and HT29R (J) cells treated or not with 20 μM 5-FU in combination with 32 μM hypoxanthine (Hyp) or 5.6 μM thymidine (Thym) in the presence of 5 μM NCT-503 for HCT-116R cells or in a medium lacking ser/gly for 48 h. Non-treated cells were used as a reference. One-way ANOVA with Tukey's *post hoc* test (n = 3).

(K) Effects of hypoxanthine supplementation on 5-FU- induced DNA damage accumulation under NCT-503 treatment in HCT-116R cells. Cells were grown either in the presence of 5 μM NCT-503 and treated or not with 20 μM 5-FU and 32 μM Hyp for 48 h before analyzing γH2AX levels from nuclear compartments.

(L) Effects of hypoxanthine supplementation on 5-FU-induced DNA damage accumulation under ser/gly starvation in HT29R cells. Cells were grown in a medium containing or lacking ser/gly and treated or not with 20 μM 5-FU and 32 μM Hyp for 48 h before analyzing the γH2AX levels from nuclear compartments. The images are representative of at least three independent experiments.

(M and N) Surviving fraction of 5-FU-resistant CRC cells treated with 5-FU in presence or absence of lometrexol (LMX). HCT-116R (M) and HT29R (N) cells were treated with/without 20 μM 5-FU and 50 nM LMX for 48 h. One-way ANOVA with Tukey's *post hoc* test (n = 3). Each dot represents a single experiment. Data are represented as mean ± standard error of the mean of at least three independent experiments. ns, not significant. *p < 0.05, **p < 0.01, ***p < 0.001.

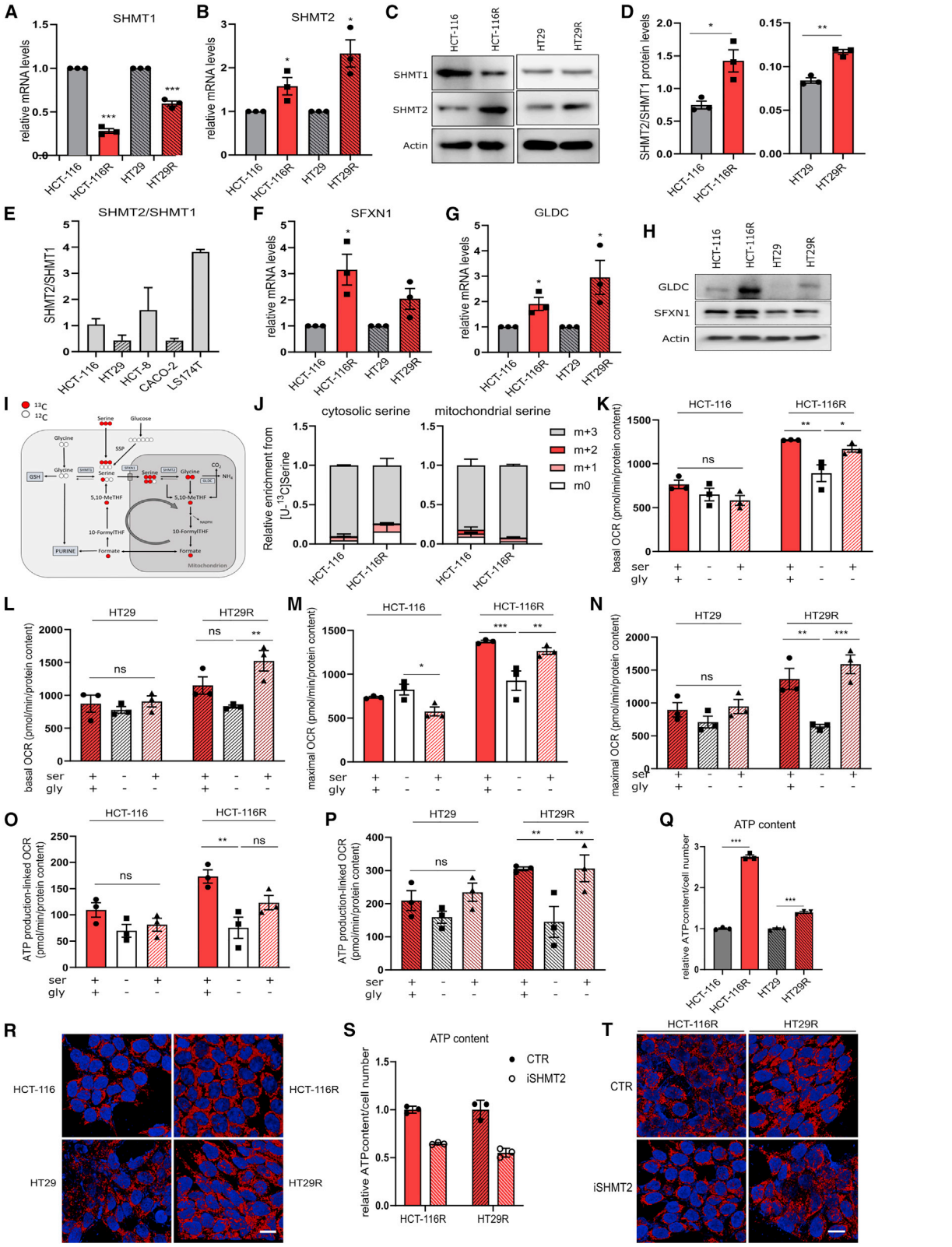

(legend on next page)

impair tumor growth (Tajan et al., 2021) and potentiate anticancer drug efficacy (Ross et al., 2017). Indeed, serine can drive different drug resistance strategies, such as maintaining intracellular antioxidant capacity (Zaal et al., 2017) or the sustaining of nucleotide biosynthesis to prevent DNA damage response (Montrose et al., 2021).

In this study, we demonstrate that interfering with serine availability potentiates the antitumor effects of 5-FU both in *in vitro* and *in vivo* CRC models. We found that increased serine use is a driving adaptation underpinning 5-FU resistance in CRC. Noteworthy, serine metabolism is under the regulation of several genetic and epigenetic modulators (Geeraerts et al., 2021), implying that different resistant clones may adopt distinct strategies to meet serine dependency according to the mutational background of the parental cells. Several regulatory mechanisms have been identified for PHGDH, including gene amplification (Locasale et al., 2011; Possemato et al., 2011), spliceosome mutations (Brian Brian Dalton et al., 2019), transcriptional regulation (DeNicola et al., 2015; Li et al., 2021; Ou et al., 2015; Riscal et al., 2016), and protein degradation (Zhang et al., 2017), resulting in high intra- and inter-tumor heterogeneity in PHGDH levels (Rossi et al., 2022; Zhang et al., 2017). The broad spectrum of experimental models described in the literature illustrates a complex interplay of multiple factors regulating serine metabolism. In our experimental model, HCT-116R cells increase SSP enzyme expression, while HT29R cells increase exogenous serine consumption. We identified p53 status and consequent MDM2 levels as key elements governing the differential response to increased serine demand during the acquisition of 5-FU resistance. However, other factors, such as activating KRAS mutations (Maddocks et al., 2017), may contribute to the differential adaptive response.

Interestingly, our data demonstrate that, regardless of the serine feeder strategy, compartmentalization of serine metabolism inside the mitochondria is the main mechanism supporting 5-FU resistance and is a common adaptation in all the analyzed 5-FU-resistant clones. The fate of serine-derived carbons is imposed by differential compartmentalization of the multiple OCM components (Li and Ye, 2020). Indeed, although cytosolic (SHMT1) and mitochondrial (SHMT2) isoforms of SHMT catalyze an equivalent biochemical reaction, they support different functions in tumor cells. Mitochondrial serine catabolism is the principal source of one-carbon units and glycine for *de novo* purine synthesis and is a major source of NADPH (Ducker et al., 2016). Besides, SHMT2 also carries OCM-independent roles in mitochondrial functionality by regulating mitochondrial respiration complexes subunits (Lucas et al., 2018; Minton et al., 2018; Morscher et al., 2018). Interestingly, the mitochondrial branch of OCM is upregulated in several human cancers, supporting cell proliferation and malignancy (Nilsson et al., 2014). SHMT2, methylenetetrahydrofolate dehydrogenase (MTHFD2), aldehyde dehydrogenase 1 family member L2, and methylenetetrahydrofolate dehydrogenase 1 like enzymes are overexpressed in CRC tissues compared with normal ones and participate in cancer progression (Agarwal et al., 2019; Miyo et al., 2017). Interestingly, mitochondrial OCM enzymes SHMT2 and MTHFD2 emerged as key determinants of the response to methotrexate (Vazquez et al., 2013), indicating their implication in the cellular response to antimetabolite drugs. Moreover, SHMT1/2 inhibition increases the antileukemic effect of methotrexate in a mouse model of NOTCH1-driven T cell acute lymphoblastic leukemia (T-ALL) and in a patient-derived T-ALL xenograft and is effective in increasing sensitivity of methotrexate-resistant human T-ALL cells (García-Cañaveras et al., 2021).

Here we demonstrate that a shift toward mitochondrial serine metabolism promotes 5-FU resistance in CRC by supporting purine nucleotide biosynthesis and allowing resistant cells to prevent the accumulation of drug-induced DNA damage. Mitochondrial compartmentalization of OCM supports 5-FU resistance by (1) promoting the synthesis of purine nucleotides to prevent DNA damage accumulation and (2) decreasing cytosolic CH_2-THF, thereby leading to reduced formation of the inhibitory ternary complex on TS by 5-FU derivatives.

Accordingly, the metabolomic analysis revealed that 5-FU resistant cells increase the flux toward the *de novo* purine

Figure 6. SHMT1-2 balance drives 5-FU resistance by leading mitochondrial serine degradation

(A and B) SHMT1/2 mRNA levels in 5-FU-resistant and sensitive CRC cell lines Student's t test (n = 3).

(C) SHMT1-SHMT2 protein levels in 5-FU-resistant and sensitive CRC cell lines. The image is representative of three independent experiments.

(D) SHMT2/1 protein levels in 5-FU-resistant and -sensitive CRC cells.

(E) SHMT2/1 mRNA levels in CRC cell lines. SHMT1 and SHMT2 gene expression was analyzed by quantitative RT-PCR and reported as the SHMT2/SHMT1 ratio (n = 3).

(F and G) SFXN1 and GLDC mRNA levels in 5-FU-resistant CRC cell lines. Student's t test (n = 3).

(H) SFXN1 and GLDC protein levels in 5-FU-resistant and -sensitive CRC cell lines. Actin was used as loading control. The image is representative of three independent experiments.

(I) Schematic representation of the tracing strategy to follow serine exploitation in cytosolic and mitochondrial compartments.

(J) Mitochondrial and cytosolic isotope composition of serine in HCT-116 and HCT-116R cells after 24 h of incubation with culture medium containing [U-^{13}C]-serine. two-way ANOVA with Sidak's *post hoc* test (n = 3).

(K–P) OCR in 5-FU-resistant CRC cell lines. Cells were incubated in a medium containing ser/gly, lacking ser/gly, or lacking only glycine for 16 h. OCR was measured in real time and normalized on protein levels. Basal (K, L), maximal (M, N), and ATP-linked (O, P) respiration was calculated by measuring the OCR after the administration of specific inhibitors. two-way ANOVA with Tukey's *post hoc* test (n = 8).

(Q) Intracellular ATP content in 5-FU-resistant and -sensitive CRC cell lines.

(R) Mitochondrial morphology in 5-FU-resistant and -sensitive CRC cell lines.

(S) Intracellular ATP content in SHMT2-silenced 5-FU-resistant CRC cells.

(T) Mitochondrial morphology in SHMT2-silenced 5-FU-resistant CRC cells.

(R and T) Confocal fluorescence microscopy images of cells stained with TMRE (red). Hoechst was used to stain nuclei (blue) (original magnification, ×63; scale bar, 5 μm). Images are representative of three independent experiments. (A–S) Each dot represents a single experiment. Data are represented as mean ± standard error of the mean of at least three independent experiments. ns, not significant. *p < 0.05, **p < 0.01, ***p < 0.001.

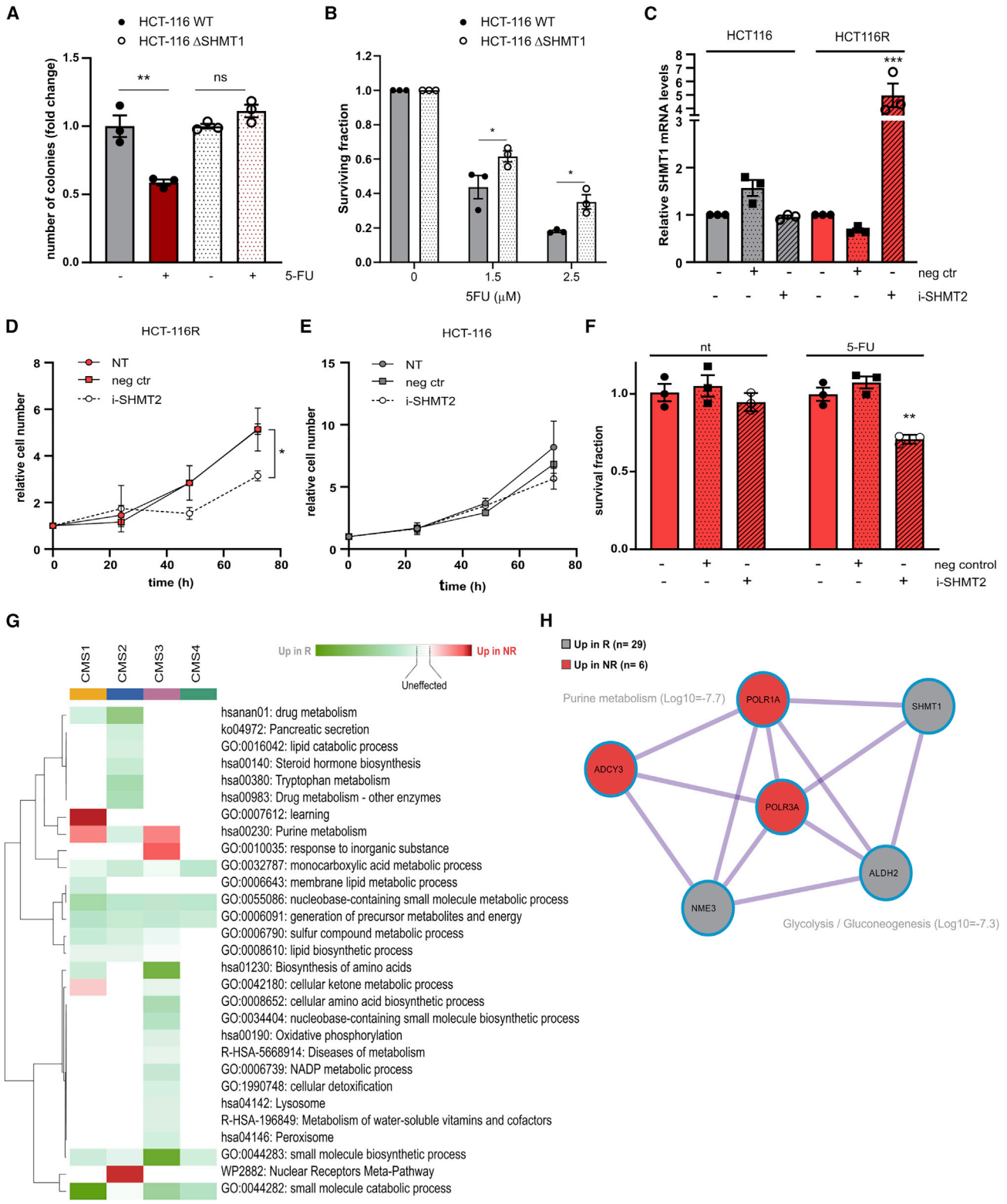

Figure 7. Modulating SHMT1/SHMT2 balance in CRC cells is effective in reversing 5-FU susceptibility

(A) Surviving fraction of HCT-116 WT and HCT-116 ΔSHMT1 cells treated with 5-FU for 48 h. Non-treated cells were used as a reference. Two-way ANOVA with Sidak's *post hoc* test (n = 3).

(legend continued on next page)

synthesis, while pyrimidine biosynthesis resulted impaired. This is in accordance with recent results demonstrating that purine, but not pyrimidine, biosynthesis supports radiation resistance in glioblastoma by promoting DNA repair (Zhou et al., 2020).

In addition, the close link between cytosolic CH_2THF accessibility and 5-FU efficacy is demonstrated by the clinical success of the 5-FU modulator leucovorin (LV, 5′-formyltetrahydrofolate), which acts by expanding the intracellular pool of 5-10-CH_2-THF to enhance the antitumor activity of 5-FU. The administration of LV in combination with 5-FU in patients with CRC increases 5-10-CH_2-THF intracellular levels (Porcelli et al., 2011) and maintains longer and stronger TS inhibition than 5-FU treatment alone (Peters et al., 1994). However, LV is ineffective in potentiating drug response in patients with 5-FU-resistant advanced CRC (van Groeningen et al., 1989).

The relevance of these results is further confirmed in clinical settings. By investigating the expression of metabolic enzymes in R and NR patients subjected to 5-FU-based therapies, we observed an increase in the expression of purine metabolism enzymes in NR patients belonging to the CMS3 and CMS1 groups. The CMS1 is typically associated with impaired DNA mismatch repair and loss of tumor suppressor function with a poor prognosis after relapse (Guinney et al., 2015). Conversely, the CMS3, also known as the metabolic subtype, is typically characterized by chromosomal instability and an overall enhancement in metabolic pathways (Guinney et al., 2015). A striking feature is that purine metabolism is enriched in NR patients irrespective of the two subgroups' distinctive mutational and genetic landscapes. This suggests that the metabolic rewiring here described is a major step in establishing chemotherapy resistance in 5-FU-based therapeutic settings. This adaptation is determined by the specific mechanism of action of the drug and is independent of other modified signaling pathways and the genetic profile of the tumor.

Our results support a possible approach to overcome drug resistance by exploiting the combination of 5-FU treatment with specific SHMT2 inhibitors. Importantly, the recent determination of the specific SHMT1/2 kinetic parameters highlighted interesting differences between the two isoforms that could be exploited to generate isoform-selective inhibitors (Scaletti et al., 2019; Tramonti et al., 2018). Our data, together with the possibility of selectively targeting SHMT2, pave the way for new therapeutic options against 5-FU resistance in CRC.

Limitation of the study

In this study, we discovered that SHMT2-mediated mitochondrial compartmentalization of serine metabolism supports the acquisition of 5-FU chemoresistance in CRC. For this study, we used several cell lines characterized by different expression levels of PHGDH and two distinct *in vivo* models revealing an overall correlation between *in vivo* and *in vitro* settings. However, some results observed in *in vitro* experiments were not recapitulated in *in vivo* settings owing to the great nutritional and signaling differences between the two experimental conditions. Our findings were further validated in CRC cancer patients' cohort selected from the TCGA-COADREAD dataset for the response to 5-FU-based therapies. However, considering the great heterogeneity in PHGDH differential expression and serine auxotrophy observed in human tumors, further studies in patient-derived tissues need to be conducted to provide more reliable conclusions.

STAR★METHODS

Detailed methods are provided in the online version of this paper and include the following:

- KEY RESOURCES TABLE
- RESOURCE AVAILABILITY
  - Lead contact
  - Materials availability
  - Data and code availability
- EXPERIMENTAL MODEL AND SUBJECT DETAILS
  - Cell lines
  - Mouse models
- METHOD DETAILS
  - Protein extraction and Western blot analysis
  - Real-Time PCR
  - RNAi transfection
  - Viability assay
  - Proliferation assay
  - Colony forming assay
  - Radioactive assays
  - CO_2 production
  - Liquid chromatography–mass spectrometry (LC–MS)
  - Gas chromatography-mass spectrometry (GC–MS)
  - Cytosolic and mitochondrial fractions isolation
  - Seahorse analysis
  - Intracellular ATP quantification

(B) Colony formation potential of HCT-116 WT and HCT-116 ΔSHMT1 cells. HCT-116 WT and HCT-116 ΔSHMT1 cells were grown either in the absence or presence of 1.5 μM 5-FU for 24 h before seeding them in new dishes and incubating for at least 10 days. Colonies were stained with crystal violet dye. Colonies number is reported using non-treated parental cells as a comparator. One-way ANOVA with Dunnett's *post hoc* test (n = 3).
(C) SHMT1 mRNA levels in HCT-116 and HCT-116R after SHMT2 silencing. Cells were transfected with SHMT2-targeting small interfering RNA (siRNA) or negative control and SHMT1 mRNA level evaluated by quantitative RT-PCR using scramble cells as a reference. One-way ANOVA with Sidak's *post hoc* test (n = 3).
(D and E) HCT-116 and HCT-116R cells proliferation following SHMT2 silencing. HCT-116R (D) and HCT-116 (E) cells were transfected with SHMT2-targeting siRNA or negative control. Cell number was assessed every 24 h. Two-way ANOVA with Tukey's *post hoc* test (n = 3).
(F) Survival fraction of SHMT2-silenced HCT-116R cells under 5-FU treatment. Cells were transfected with SHMT2-targeting siRNA or negative control and were let to proliferate in a medium containing 20 μM 5-FU for 48 h. Two-way ANOVA with Sidak's *post hoc* test (n = 3).
(G) Heatmap summarizing metabolic pathway enrichment analysis in TCGA-COADREAD, comparing R versus NR patients according to CMS classification.
(H) Molecular complex detection (MCODE) protein network analysis for enriched metabolic pathways comparing R versus NR CMS1 patients.
(I) SHMT1 RNA levels in R and NR CMS1 patients. Student's t test. Each dot represents a single patient. Data are represented as mean ± standard error of the mean of at least three independent experiments. Ns, not significant. *p < 0.05, **p < 0.01, ***p < 0.001.

- Confocal microscopy image acquisition
- *In vivo* ultrasound imaging
- TCGA-COADREAD dataset analysis

● QUANTIFICATION AND STATISTICAL ANALYSIS

SUPPLEMENTAL INFORMATION

Supplemental information can be found online at https://doi.org/10.1016/j.celrep.2022.111233.

ACKNOWLEDGMENTS

The authors acknowledge Prof. J.D. Rabinowitz (Princeton University) and Prof. G. Russo (University of Naples, Federico II) for the kind gift of HCT-116-ΔSHMT1 cells and p53$^{-/-}$ HCT-116 cells, respectively. The authors thank Francesco Maria del Re, Alessandra Traviglia, and Sara Roccabianca for the help in performing the experiments. This research was supported by the University of Florence (Fondo ex-60%), the project "Development of VEGFR/Tubulin and Efflux Pump inhibitors loaded on stimuli-responsive cell membrane coated nanocarriers for the treatment of metastatic" funded by the MIUR Progetti di Ricerca di Rilevante Interesse Nazionale (PRIN)-Bando 2020 (grant no. 2020239N53), and by the Associazione Italiana Ricerca sul Cancro (AIRC) (project code: 19515). E. Pranzini is supported by an AIRC fellowship (project code: 24132). E. Pardella is supported by an AIRC fellowship for Italy (project code 26599). We thank Simone Vogogna for the financial support. Graphical representations were generated by Biorender.com.

AUTHOR CONTRIBUTIONS

Conception and design: E. Pranzini, P.C, P.P., and M.L.T.; Collection of data: E. Pranzini, E. Pardella, L.M., A.L., and I.N.; Analysis and interpretation of data: E. Pranzini, L.M., O.D.K.M., P.P., and M.L.T.; Technical support: I.N., M.P., T.Z., T.L., A and.S.; Writing and/or revision of the manuscript: E. Pranzini, E. Pardella., L.M., L.S., V.C., P. Cirri, P. Chiarugi, P.P., and M.L.T. Funding acquisition: A.C., P. Cirri, P. Chiarugi, G.R., A.A., O.D.K.M., P.P., and M.L.T.; Study supervision, P.P. and M.L.T. All authors discussed the results and contributed to the final manuscript.

DECLARATION OF INTERESTS

The authors declare that they have no conflict of interest.

Received: August 9, 2021
Revised: March 31, 2022
Accepted: July 27, 2022
Published: August 16, 2022

REFERENCES

Agarwal, S., Behring, M., Hale, K., Al Diffalha, S., Wang, K., Manne, U., and Varambally, S. (2019). MTHFD1L, A folate cycle enzyme, is involved in progression of colorectal cancer. Transl. Oncol. *12*, 1461–1467. https://doi.org/10.1016/j.tranon.2019.07.011.

Ahmed, D., Eide, P.W., Eilertsen, I.A., Danielsen, S.A., Eknæs, M., Hektoen, M., Lind, G.E., and Lothe, R.A. (2013). Epigenetic and genetic features of 24 colon cancer cell lines. Oncogenesis *2*, e71. https://doi.org/10.1038/oncsis.2013.35.

Anderson, D.D., Quintero, C.M., and Stover, P.J. (2011). Identification of a de novo thymidylate biosynthesis pathway in mammalian mitochondria. Proc. Natl. Acad. Sci. USA *108*, 15163–15168. https://doi.org/10.1073/pnas.1103623108.

Bao, X., Ong, R.S.-E., Goldberger, o., Peng, J., Sharma, R., Thompson, D.A., Vafai, S.B., Cox, A.G., Marutani, E., Ichinoseet, F., et al. (2016). Mitochondrial Dysfunction Remodels One-Carbon Metabolism in Human Cells. https://doi.org/10.7554/eLife.10575.001.

Dalton, W.B., Helmenstine, E., Walsh, N., Gondek, L.P., Kelkar, D.S., Read, A., Natrajan, R., Christenson, E.S., Roman, B., Das, S., et al. (2019). Hotspot SF3B1 mutations induce metabolic reprogramming and vulnerability to serine deprivation. J. Clin. Invest. *129*, 4708–4723. https://doi.org/10.1172/JCI125022.

Bröer, S., and Bröer, A. (2017). Amino acid homeostasis and signalling in mammalian cells and organisms. Biochem. J. *474*, 1935–1963. https://doi.org/10.1042/BCJ20160822.

Buescher, J.M., Antoniewicz, M.R., Boros, L.G., Burgess, S.C., Brunengraber, H., Clish, C.B., DeBerardinis, R.J., Feron, O., Frezza, C., Ghesquiere, B., et al. (2015). A roadmap for interpreting 13 C metabolite labeling patterns from cells. Curr. Opin. Biotechnol. *34*, 189–201. https://doi.org/10.1016/j.copbio.2015.02.003.

Calvo, S.E., Clauser, K.R., and Mootha, V.K. (2016). MitoCarta2.0: an updated inventory of mammalian mitochondrial proteins. Nucleic Acids Res. *44*, D1251–D1257. https://doi.org/10.1093/nar/gkv1003.

Corcoran, C.C., Grady, C.R., Pisitkun, T., Parulekar, J., and Knepper, M.A. (2017). From 20th century metabolic wall charts to 21st century systems biology: database of mammalian metabolic enzymes. Am J. Physiol Renal. Physiol. *312*, F533–F542. https://doi.org/10.1152/ajprenal.00601.2016.

Davidson, D., Coulombe, Y., Martinez-Marignac, V.L., Amrein, L., Grenier, J., Hodkinson, K., Masson, J.-Y., Aloyz, R., and Panasci, L. (2012). Irinotecan and DNA-PKcs inhibitors synergize in killing of colon cancer cells. Invest. New Drugs *30*, 1248–1256. https://doi.org/10.1007/s10637-010-9626-9.

DeNicola, G.M., Chen, P.-H., Mullarky, E., Sudderth, J.A., Hu, Z., Wu, D., Tang, H., Xie, Y., Asara, J.M., Huffman, K.E., et al. (2015). NRF2 regulates serine biosynthesis in non-small cell lung cancer. Nat. Genet. *47*, 1475–1481. https://doi.org/10.1038/ng.3421.

Denise, C., Paoli, P., Calvani, M., Taddei, M.L., Giannoni, E., Kopetz, S., Kazmi, S.M.A., Pia, M.M., Pettazzoni, P., Sacco, E., et al. (2015). 5-fluorouracil resistant colon cancer cells are addicted to OXPHOS to survive and enhance stem-like traits. Oncotarget *6*, 41706–41721. https://doi.org/10.18632/oncotarget.5991.

Desbats, M.A., Giacomini, I., Prayer-Galetti, T., and Montopoli, M. (2020). Metabolic plasticity in chemotherapy resistance. Front. Oncol. *10*, 281. https://doi.org/10.3389/fonc.2020.00281.

Ducker, G.S., and Rabinowitz, J.D. (2017). One-carbon metabolism in health and disease. Cell Metab. *25*, 27–42. https://doi.org/10.1016/j.cmet.2016.08.009.

Ducker, G.S., Chen, L., Morscher, R.J., Ghergurovich, J.M., Esposito, M., Teng, X., Kang, Y., and Rabinowitz, J.D. (2016). Reversal of cytosolic one-carbon flux compensates for loss of the mitochondrial folate pathway. Cell Metab *23*, 1140–1153. https://doi.org/10.1016/j.cmet.2016.04.016.

Ducker, G.S., Ghergurovich, J.M., Mainolfi, N., Suri, V., Jeong, S.K., Hsin-Jung Li, S., Friedman, A., Manfredi, M.G., Gitai, Z., Kim, H., and Rabinowitz, J.D. (2017). Human SHMT inhibitors reveal defective glycine import as a targetable metabolic vulnerability of diffuse large B-cell lymphoma. Proc. Natl. Acad. Sci. USA *114*, 11404–11409. https://doi.org/10.1073/pnas.1706617114.

Fan, T.W.M., Bruntz, R.C., Yang, Y., Song, H., Chernyavskaya, Y., Deng, P., Zhang, Y., Shah, P.P., Beverly, L.J., Qi, Z., et al. (2019). De novo synthesis of serine and glycine fuels purine nucleotide biosynthesis in human lung cancer tissues. J. Biol. Chem. *294*, 13464–13477. https://doi.org/10.1074/jbc.RA119.008743.

Franken, N.A.P., Rodermond, H.M., Stap, J., Haveman, J., and van Bree, C. (2006). Clonogenic assay of cells in vitro. Nat. Protoc. *1*, 2315–2319. https://doi.org/10.1038/nprot.2006.339.

García-Cañaveras, J.C., Lancho, O., Ducker, G.S., Ghergurovich, J.M., Xu, X., da Silva-Diz, V., Minuzzo, S., Indraccolo, S., Kim, H., Herranz, D., and Rabinowitz, J.D. (2021). SHMT inhibition is effective and synergizes with methotrexate in T-cell acute lymphoblastic leukemia. Leukemia *35*, 377–388. https://doi.org/10.1038/s41375-020-0845-6.

Geeraerts, S.L., Heylen, E., De Keersmaecker, K., and Kampen, K.R. (2021). The ins and outs of serine and glycine metabolism in cancer. Nat. Metab. *3*, 131–141. https://doi.org/10.1038/s42255-020-00329-9.

Guinney, J., Dienstmann, R., Wang, X., de Reyniès, A., Schlicker, A., Soneson, C., Marisa, L., Roepman, P., Nyamundanda, G., Angelino, P., et al. (2015). The consensus molecular subtypes of colorectal cancer. Nat. Med. *21*, 1350–1356. https://doi.org/10.1038/nm.3967.

Humpton, T.J., Hock, A.K., Maddocks, O.D.K., and Vousden, K.H. (2018). p53-mediated adaptation to serine starvation is retained by a common tumour-derived mutant. Cancer Metab *6*, 18. https://doi.org/10.1186/s40170-018-0191-6.

Kory, N., Wyant, G.A., Prakash, G., Uit de Bos, J., Bottanelli, F., Pacold, M.E., Chan, S.H., Lewis, C.A., Wang, T., Keys, H.R., et al. (2018). SFXN1 is a mitochondrial serine transporter required for one-carbon metabolism. Science *362*. https://doi.org/10.1126/science.aat9528.

Labuschagne, C.F., van den Broek, N.J.F., Mackay, G.M., Vousden, K.H., and Maddocks, O.D.K. (2014). Serine, but not glycine, supports one-carbon metabolism and proliferation of cancer cells. Cell Rep. *7*, 1248–1258. https://doi.org/10.1016/j.celrep.2014.04.045.

Leary, M., Heerboth, S., Lapinska, K., and Sarkar, S. (2018). Sensitization of drug resistant cancer cells: a matter of combination therapy. Cancers *10*, 483. https://doi.org/10.3390/cancers10120483.

Li, A.M., and Ye, J. (2020). Reprogramming of serine, glycine and one-carbon metabolism in cancer. Biochim. Biophys. Acta, Mol. Basis Dis. *1866*, 165841. https://doi.org/10.1016/j.bbadis.2020.165841.

Li, X., Gracilla, D., Cai, L., Zhang, M., Yu, X., Chen, X., Zhang, J., Long, X., Ding, H.F., and Yan, C. (2021). ATF3 promotes the serine synthesis pathway and tumor growth under dietary serine restriction. Cell Rep. *36*, 109706. https://doi.org/10.1016/j.celrep.2021.109706.

Locasale, J.W., Grassian, A.R., Melman, T., Lyssiotis, C.A., Mattaini, K.R., Bass, A.J., Heffron, G., Metallo, C.M., Muranen, T., Sharfi, H., et al. (2011). Phosphoglycerate dehydrogenase diverts glycolytic flux and contributes to oncogenesis. Nat. Genet. *43*, 869–874. https://doi.org/10.1038/ng.890.

Longley, D.B., Harkin, D.P., and Johnston, P.G. (2003). 5-Fluorouracil: mechanisms of action and clinical strategies. Nat. Rev. Cancer *3*, 330–338. https://doi.org/10.1038/nrc1074.

Lucas, S., Chen, G., Aras, S., and Wang, J. (2018). Serine catabolism is essential to maintain mitochondrial respiration in mammalian cells. Life Science Alliance *1*, e201800036. https://doi.org/10.26508/lsa.201800036.

Maddocks, O.D.K., Berkers, C.R., Mason, S.M., Zheng, L., Blyth, K., Gottlieb, E., and Vousden, K.H. (2013). Serine starvation induces stress and p53-dependent metabolic remodelling in cancer cells. Nature *493*, 542–546. https://doi.org/10.1038/nature11743.

Maddocks, O.D.K., Labuschagne, C.F., Adams, P.D., and Vousden, K.H. (2016). Serine metabolism supports the methionine cycle and DNA/RNA methylation through de novo ATP synthesis in cancer cells. Mol. Cell *61*, 210–221. https://doi.org/10.1016/j.molcel.2015.12.014.

Maddocks, O.D.K., Athineos, D., Cheung, E.C., Lee, P., Zhang, T., van den Broek, N.J.F., Mackay, G.M., Labuschagne, C.F., Gay, D., Kruiswijk, F., et al. (2017). Modulating the therapeutic response of tumours to dietary serine and glycine starvation. Nature *544*, 372–376. https://doi.org/10.1038/nature22056.

Mah, L.-J., El-Osta, A., and Karagiannis, T.C. (2010). γH2AX: a sensitive molecular marker of DNA damage and repair. Leukemia *24*, 679–686. https://doi.org/10.1038/leu.2010.6.

Millard, P., Delépine, B., Guionnet, M., Heuillet, M., Bellvert, F., and Létisse, F. (2019). IsoCor: isotope correction for high-resolution MS labeling experiments. Bioinformatics *35*, 4484–4487. https://doi.org/10.1093/bioinformatics/btz209.

Minton, D.R., Nam, M., McLaughlin, D.J., Shin, J., Bayraktar, E.C., Alvarez, S.W., Sviderskiy, V.O., Papagiannakopoulos, T., Sabatini, D.M., Birsoy, K., and Possemato, R. (2018). Serine catabolism by SHMT2 is required for proper mitochondrial translation Initiation and maintenance of Formylmethionyl-tRNAs. Mol. Cell *69*, 610–621.e5. https://doi.org/10.1016/j.molcel.2018.01.024.

Miyo, M., Konno, M., Colvin, H., Nishida, N., Koseki, J., Kawamoto, K., Tsunekuni, K., Nishimura, J., Hata, T., Takemasa, I., et al. (2017). The importance of mitochondrial folate enzymes in human colorectal cancer. Oncol. Rep. *37*, 417–425. https://doi.org/10.3892/or.2016.5264.

Montrose, D.C., Saha, S., Foronda, M., McNally, E.M., Chen, J., Zhou, X.K., Ha, T., Krumsiek, J., Buyukozkan, M., Verma, A., et al. (2021). Exogenous and endogenous sources of serine contribute to colon cancer metabolism, growth, and resistance to 5-fluorouracil. Cancer Res. *81*, 2275–2288. https://doi.org/10.1158/0008-5472.CAN-20-1541.

Morscher, R.J., Ducker, G.S., Li, S.H.J., Mayer, J.A., Gitai, Z., Sperl, W., and Rabinowitz, J.D. (2018). Mitochondrial translation requires folate-dependent tRNA methylation. Nature *554*, 128–132. https://doi.org/10.1038/nature25460.

Newman, A.C., and Maddocks, O.D.K. (2017). One-carbon metabolism in cancer. Br. J. Cancer *116*, 1499–1504. https://doi.org/10.1038/bjc.2017.118.

Nilsson, R., Jain, M., Madhusudhan, N., Sheppard, N.G., Strittmatter, L., Kampf, C., Huang, J., Asplund, A., and Mootha, V.K. (2014). Metabolic enzyme expression highlights a key role for MTHFD2 and the mitochondrial folate pathway in cancer. Nat. Commun. *5*, 3128. https://doi.org/10.1038/ncomms4128.

Nonnenmacher, Y., Palorini, R., d'Herouël, A.F., Krämer, L., Neumann-Schaal, M., Chiaradonna, F., Skupin, A., Wegner, A., and Hiller, K. (2017). Analysis of mitochondrial metabolism in situ: combining stable isotope labeling with selective permeabilization. Metab. Eng. *43*, 147–155. https://doi.org/10.1016/j.ymben.2016.12.005.

Nonnenmacher, Y., Palorini, R., and Hiller, K. (2019). Determining compartment-specific metabolic Fluxes. Methods Mol. Biol. *1862*, 137–149. https://doi.org/10.1007/978-1-4939-8769-6_10.

Ou, Y., Wang, S.J., Jiang, L., Zheng, B., and Gu, W. (2015). p53 Protein-mediated regulation of phosphoglycerate dehydrogenase (PHGDH) is crucial for the apoptotic response upon serine starvation. J. Biol. Chem. *290*, 457–466. https://doi.org/10.1074/jbc.M114.616359.

Pacold, M.E., Brimacombe, K.R., Chan, S.H., Rohde, J.M., Lewis, C.A., Swier, L.J.Y.M., Possemato, R., Chen, W.W., Sullivan, L.B., Fiske, B.P., et al. (2016). A PHGDH inhibitor reveals coordination of serine synthesis and one-carbon unit fate. Nat. Chem. Biol. *12*, 452–458. https://doi.org/10.1038/nchembio.2070.

Pagliarini, D.J., Calvo, S.E., Chang, B., Sheth, S.A., Vafai, S.B., Ong, S.-E., Walford, G.A., Sugiana, C., Boneh, A., Chen, W.K., et al. (2008). A mitochondrial protein compendium elucidates complex I disease biology. Cell *134*, 112–123. https://doi.org/10.1016/j.cell.2008.06.016.

Park, E.Y., Dillard, A., Williams, E.A., Wilder, E.T., Pepper, M.R., and Lane, M.A. (2005). Retinol inhibits the growth of all-trans-retinoic acid-sensitive and all-trans-retinoic acid-resistant colon cancer cells through a retinoic acid receptor-independent mechanism. Cancer Res. *65*, 9923–9933. https://doi.org/10.1158/0008-5472.CAN-05-1604.

Peters, G.J., van der Wilt, C.L., van Groeningen, C.J., Smid, K., Meijer, S., and Pinedo, H.M. (1994). Thymidylate synthase inhibition after administration of fluorouracil with or without leucovorin in colon cancer patients: implications for treatment with fluorouracil. J. Clin. Oncol. *12*, 2035–2042. https://doi.org/10.1200/JCO.1994.12.10.2035.

Peters, G.J., Backus, H.H.J., Freemantle, S., van Triest, B., Codacci-Pisanelli, G., van der Wilt, C.L., Smid, K., Lunec, J., Calvert, A.H., Marsh, S., et al. (2002). Induction of thymidylate synthase as a 5-fluorouracil resistance mechanism. Biochim. Biophys. Acta *1587*, 194–205. https://doi.org/10.1016/s0925-4439(02)00082-0.

Poliaková, M., Aebersold, D.M., Zimmer, Y., and Medová, M. (2018). The relevance of tyrosine kinase inhibitors for global metabolic pathways in cancer. Mol. Cancer *17*, 27. https://doi.org/10.1186/s12943-018-0798-9.

Pollari, S., Käkönen, S.-M., Edgren, H., Wolf, M., Kohonen, P., Sara, H., Guise, T., Nees, M., and Kallioniemi, O. (2011). Enhanced serine production by bone

metastatic breast cancer cells stimulates osteoclastogenesis. Breast Cancer Res. Treat. *125*, 421–430. https://doi.org/10.1007/s10549-010-0848-5.

Porcelli, L., G Assaraf, Y., Azzariti, A., Paradiso, A., Jansen, G., and J Peters, G. (2011). The impact of folate status on the efficacy of colorectal cancer treatment. Curr. Drug Metab *12*, 975–984. https://doi.org/10.2174/138920011798062274.

Possemato, R., Marks, K.M., Shaul, Y.D., Pacold, M.E., Kim, D., Birsoy, K., Sethumadhavan, S., Woo, H.-K., Jang, H.G., Jha, A.K., et al. (2011). Functional genomics reveal that the serine synthesis pathway is essential in breast cancer. Nature *476*, 346–350. https://doi.org/10.1038/nature10350.

Pranzini, E., Pardella, E., Paoli, P., Fendt, S.-M., and Taddei, M.L. (2021). Metabolic reprogramming in anticancer drug resistance: a Focus on amino acids. Trends Cancer *7*, 682–699. https://doi.org/10.1016/j.trecan.2021.02.004.

Rinaldi, G., Pranzini, E., van Elsen, J., Broekaert, D., Funk, C.M., Planque, M., Doglioni, G., Altea-Manzano, P., Rossi, M., Geldhof, V., et al. (2021). In vivo evidence for serine biosynthesis-defined sensitivity of lung metastasis, but not of primary breast tumors, to mTORC1 inhibition. Mol. Cell *81*, 386–397.e7. https://doi.org/10.1016/j.molcel.2020.11.027.

Riscal, R., Schrepfer, E., Arena, G., Cissé, M.Y., Bellvert, F., Heuillet, M., Rambow, F., Bonneil, E., Sabourdy, F., Vincent, C., et al. (2016). Chromatin-bound MDM2 regulates serine metabolism and redox homeostasis independently of p53. Mol. Cell *62*, 890–902. https://doi.org/10.1016/j.molcel.2016.04.033.

Ross, K.C., Andrews, A.J., Marion, C.D., Yen, T.J., and Bhattacharjee, V. (2017). Identification of the serine biosynthesis pathway as a critical component of BRAF inhibitor resistance of melanoma, pancreatic, and non-small cell lung cancer cells. Mol. Cancer Ther. *16*, 1596–1609. https://doi.org/10.1158/1535-7163.MCT-16-0798.

Rossi, M., Altea-Manzano, P., Demicco, M., Doglioni, G., Bornes, L., Fukano, M., Vandekeere, A., Cuadros, A.M., Fernández-García, J., Riera-Domingo, C., et al. (2022). PHGDH heterogeneity potentiates cancer cell dissemination and metastasis. Nature *605*, 747–753. https://doi.org/10.1038/s41586-022-04758-2.

Scaletti, E., Jemth, A.-S., Helleday, T., and Stenmark, P. (2019). Structural basis of inhibition of the human serine hydroxymethyltransferase SHMT2 by antifolate drugs. FEBS Lett. *593*, 1863–1873. https://doi.org/10.1002/1873-3468.13455.

Schneider, C.A., Rasband, W.S., and Eliceiri, K.W. (2012). NIH Image to ImageJ: 25 years of image analysis. Nat. Methods *9*, 671–675. https://doi.org/10.1038/nmeth.2089.

Ser, Z., Gao, X., Johnson, C., Mehrmohamadi, M., Liu, X., Li, S., and Locasale, J.W. (2016). Targeting one carbon metabolism with an antimetabolite disrupts pyrimidine homeostasis and induces nucleotide overflow. Cell Rep. *15*, 2367–2376. https://doi.org/10.1016/j.celrep.2016.05.035.

Silva, T.C., Colaprico, A., Olsen, C., D'Angelo, F., Bontempi, G., Ceccarelli, M., and Noushmehr, H. (2016). TCGA Workflow: analyze cancer genomics and epigenomics data using Bioconductor packages. F1000Res *5*, 1542. https://doi.org/10.12688/f1000research.8923.2.

Tajan, M., Hennequart, M., Cheung, E.C., Zani, F., Hock, A.K., Legrave, N., Maddocks, O.D.K., Ridgway, R.A., Athineos, D., Suárez-Bonnet, A., et al. (2021). Serine synthesis pathway inhibition cooperates with dietary serine and glycine limitation for cancer therapy. Nat. Commun. *12*, 366. https://doi.org/10.1038/s41467-020-20223-y.

Tani, H., Ohnishi, S., Shitara, H., Mito, T., Yamaguchi, M., Yonekawa, H., Hashizume, O., Ishikawa, K., Nakada, K., and Hayashi, J.-I. (2018). Mice deficient in the Shmt2 gene have mitochondrial respiration defects and are embryonic lethal. Sci. Rep. *8*, 425. https://doi.org/10.1038/s41598-017-18828-3.

Tedeschi, P.M., Markert, E.K., Gounder, M., Lin, H., Dvorzhinski, D., Dolfi, S.C., Chan, L.L.Y., Qiu, J., DiPaola, R.S., Hirshfield, K.M., et al. (2013). Contribution of serine, folate and glycine metabolism to the ATP, NADPH and purine requirements of cancer cells. Cell Death Dis. *4*, e877. https://doi.org/10.1038/cddis.2013.393.

Tramonti, A., Nardella, C., di Salvo, M.L., Barile, A., Cutruzzolà, F., and Contestabile, R. (2018). Human cytosolic and mitochondrial serine hydroxymethyltransferase isoforms in comparison: Full kinetic characterization and substrate inhibition properties. Biochemistry *57*, 6984–6996. https://doi.org/10.1021/acs.biochem.8b01074.

van Groeningen, C.J., Peters, G.J., and Pinedo, H.M. (1989). Lack of effectiveness of combined 5-fluorouracil and leucovorin in patients with 5-fluorouracil-resistant advanced colorectal cancer. Eur. J. Cancer Clin. Oncol. *25*, 45–49. https://doi.org/10.1016/0277-5379(89)90049-7.

Vazquez, A., Markert, E.K., and Oltvai, Z.N. (2011). Serine biosynthesis with one carbon catabolism and the glycine cleavage system represents a novel pathway for ATP generation. PLoS One *6*, e25881. https://doi.org/10.1371/journal.pone.0025881.

Vazquez, A., Tedeschi, P.M., and Bertino, J.R. (2013). Overexpression of the mitochondrial folate and glycine-serine pathway: a new determinant of methotrexate selectivity in tumors. Cancer Res. *73*, 478–482. https://doi.org/10.1158/0008-5472.CAN-12-3709.

Vodenkova, S., Buchler, T., Cervena, K., Veskrnova, V., Vodicka, P., and Vymetalkova, V. (2020). 5-fluorouracil and other fluoropyrimidines in colorectal cancer: past, present and future. Pharmacol. Ther. *206*, 107447. https://doi.org/10.1016/j.pharmthera.2019.107447.

Wang, J., Kuropatwinski, K., Hauser, J., Rossi, M.R., Zhou, Y., Conway, A., Kan, J.L.C., Gibson, N.W., Willson, J.K.V., Cowell, J.K., and Brattain, M.G. (2007). Colon carcinoma cells harboring PIK3CA mutations display resistance to growth factor deprivation induced apoptosis. Mol. Cancer Ther. *6*, 1143–1150. https://doi.org/10.1158/1535-7163.MCT-06-0555.

Yang, M., and Vousden, K.H. (2016). Serine and one-carbon metabolism in cancer. Nat. Rev. Cancer *16*, 650–662. https://doi.org/10.1038/nrc.2016.81.

Zaal, E.A., Wu, W., Jansen, G., Zweegman, S., Cloos, J., and Berkers, C.R. (2017). Bortezomib resistance in multiple myeloma is associated with increased serine synthesis. Cancer Metab *5*, 7. https://doi.org/10.1186/s40170-017-0169-9.

Zecchini, V., and Frezza, C. (2017). Metabolic synthetic lethality in cancer therapy. Biochim. Biophys. Acta Bioenerg. *1858*, 723–731. https://doi.org/10.1016/j.bbabio.2016.12.003.

Zhang, N., Yin, Y., Xu, S.-J., and Chen, W.-S. (2008). 5-Fluorouracil: mechanisms of resistance and reversal strategies. Molecules *13*, 1551–1569. https://doi.org/10.3390/molecules13081551.

Zhang, W.C., Shyh-Chang, N., Yang, H., Rai, A., Umashankar, S., Ma, S., Soh, B.S., Sun, L.L., Tai, B.C., Nga, M.E., et al. (2012). Glycine decarboxylase activity drives non-small cell lung cancer tumor-initiating cells and tumorigenesis. Cell *148*, 259–272. https://doi.org/10.1016/j.cell.2011.11.050.

Zhang, B., Zheng, A., Hydbring, P., Ambroise, G., Ouchida, A.T., Goiny, M., Vakifahmetoglu-Norberg, H., and Norberg, E. (2017). PHGDH defines a metabolic subtype in lung Adenocarcinomas with poor prognosis. Cell Rep. *19*, 2289–2303. https://doi.org/10.1016/j.celrep.2017.05.067.

Zhou, Y., Zhou, B., Pache, L., Chang, M., Khodabakhshi, A.H., Tanaseichuk, O., Benner, C., and Chanda, S.K. (2019). Metascape provides a biologist-oriented resource for the analysis of systems-level datasets. Nat. Commun. *10*, 1523. https://doi.org/10.1038/s41467-019-09234-6.

Zhou, W., Yao, Y., Scott, A.J., Wilder-Romans, K., Dresser, J.J., Werner, C.K., Sun, H., Pratt, D., Sajjakulnukit, P., Zhao, S.G., et al. (2020). Purine metabolism regulates DNA repair and therapy resistance in glioblastoma. Nat. Commun. *11*, 3811. https://doi.org/10.1038/s41467-020-17512-x.

STAR★METHODS

KEY RESOURCES TABLE

REAGENT or RESOURCE	SOURCE	IDENTIFIER
Antibodies		
PHGDH	Thermo Fisher Scientific	Cat# PA5-54360; RRID: AB_2645502
PSAT-1	Thermo Fisher Scientific	Cat# PA522124; RRID: AB_11153526
PSPH	Thermo Fisher Scientific	Cat# PA596863; RRID: AB_2808665
NRF2	Genetex	Cat# GTX103322 RRID:AB_1950993
p21	SantaCruz Biotecnology	Cat# sc-271610; RRID: AB_10647231
MDM2	SantaCruz Biotecnology	Cat# sc-965; RRID: AB_627920
p53	SantaCruz Biotecnology	Cat# sc-126; RRID: AB_628082
phospho-H2AX	Abcam	Cat# 81299; RRID: AB_1640564
H3	Cell Signaling	Cat# 9715; RRID:AB_331563
SHMT1	Thermo Fisher Scientific	Cat# PA5-54758; RRID: AB_2647280
SHMT2	SantaCruz Biotecnology	Cat# sc-390641; RRID:AB_2920890
SFXN1	Thermo Fisher Scientific	Cat# PA588887; RRID: AB_2805197
GLDC	Thermo Fisher Scientific	Cat# PA597294; RRID: AB_2809096
Tubulin	SantaCruz Biotecnology	Cat# sc-5286; RRID: AB_628411
GAPDH	SantaCruz Biotecnology	Cat# sc-48166; RRID: AB_783595
β-Actin	SantaCruz Biotecnology	Cat# sc-47778; RRID: AB_626632
Anti-rabbit	Santa Cruz Biotechology	Cat# sc-2357; RRID: AB_628497
anti-mouse	Santa Cruz Biotechology	Cat# sc-2005; RRID: AB_631736
Chemicals, peptides, and recombinant proteins		
Methanol	Sigma	Cat# 900688-1
Acetonitrile	Sigma	Cat# 34851
Ethanol	Merck Sigma	Cat# 02870
Dimethyl sulfoxide (DMSO)	Merck Sigma	Cat# 472301
Phosphate Buffer Saline w/o Ca w/o Mg (PBS)	EuroClone	Cat# ECB4004L
Dulbecco's modified Eagle's medium (DMEM)	Merck Sigma	Cat# D5671
Trypsin EDTA	EuroClone	Cat# ECM0920D
Fetal bovine serum (FBS)	EuroClone	Cat# ECS0180L
Penicillin/Streptomicin 100X	EuroClone	Cat# ECB3001D
L-Glutamine Solution 200 mM	Merck Sigma	Cat# G7513
MEM medium	Gibco	Cat# 21090
MEM vitamins	Merck Sigma	Cat# M6895
D-glucose	Merck Sigma	Cat# G8644
5-Fluorouracil (5-FU)	Merck Sigma	Cat# F6627
MycoAlert Mycoplasma Detection Kit	Lonza	Cat# LOLT07218
NCT-503 (for *in vitro* experiements)	Merck Sigma	Cat# SML1659
NCT-503 (for *in vivo* experiments)	DivBio Science	Cat# S8619
Kollisolv PEG E300	Merck Sigma	Cat# 91462
hydroxypropyl-β-cyclodextrin	Merck Sigma	Cat# H107
Protease Inhibitor Cocktail	Merck Sigma	Cat# P8340
Phosphatase Inhibitor Cocktail	Merck Sigma	Cat# P5726
Pierce BCA Protein Assay Kit	Merck Sigma	Cat# BCA1
Precast polyacrylamide gel 4-20% MP TGX	Merck Sigma	Cat# 4568096

(*Continued on next page*)

Continued

REAGENT or RESOURCE	SOURCE	IDENTIFIER
Trans-Blot Turbo Midi PVDF membranes	BioRad	Cat# 1704157
Non-fat dry milk	SantaCruz Biotechnology	Cat# sc-2325
All Blue Prestained Protein Standards	BioRad	Cat# 1610373
Clarity Western ECL Substrate	BioRad	Cat# 1705061
Lipofectamine RNAiMAX	Thermo Fisher Scientific	Cat# 13778-150
Opti-MEM	GIBCO	Cat# 31985062
Crystal Violet	Merck Sigma	Cat# 548629
Hypoxanthine	Merck Sigma	Cat# H9377
Lometroxol hydrate	Merck Sigma	Cat# SML-0040
Thymidine	Merck Sigma	Cat# T1895
Pemetrexed	Merck Sigma	Cat# SML1490
DL-Serine	Merck Sigma	Cat# S5386
Glycine	Merck Sigma	Cat# G8790
[1-2^{14}C]-Serine	Perkin Elmer	Cat# NEC853050UC
[1-^{14}C]-Glucose	Perkin Elmer	Cat# NEC043X
[6-^{14}C]-Glucose	Perkin Elmer	Cat# NEC045X050UC
[U-^{13}C]-D-Glucose	Cambrige Isotope laboratories	Cat# CLM-1396-1
[U-^{13}C]-Serine	Cambrige Isotope laboratories	Cat# CLM-1572-PK
DL-Norvaline	Merck Sigma	Cat# 53721
Methoxyamine	Merck Sigma	Cat# 226904
Pyridine	Merck Sigma	Cat# 270970
N-(tert-butyldimethylsilyl)-N-methyl-trifluoroacetamide	Merck Sigma	Cat# 375934
Digitonin	Merck Sigma	Cat# D141
TMRE probe	Thermo Fisher Scientific	Cat# T669
Hoechst	Thermo Fisher Scientific	Cat# 62249
Critical commercial assays		
RNeasy Plus Mini Kit	Qiagen	Cat# 74134
QuantiTect cDNA Reverse Transcription Kit	Qiagen	Cat# 205311
QuantiFast SYBR Green PCR kit	Qiagen	Cat# 204054
Seahorse XF Cell Mito Stress Kit	Agilent Technologies	Cat# 103015-100
ATP Detection kit-luminescence Assay	BioVision	Cat# CAY-700410-1
Deposited data		
Original western blot images	This paper; Mendeley Data	https://data.mendeley.com/datasets/hzbdfyz367/1
The Cancer Genome Atlas (TGCA)	Open source	http://firebrowse.org
Experimental models: Cell lines		
HCT-116	ATCC	Cat# CCL-247
HT29	ATCC	Cat# HTB-38
HCT8	ATCC	Cat# CCL-244
CACO-2	ATCC	Cat# HTB-37
DLD-1	ATCC	Cat# CCL-221
LoVo	ATCC	Cat# CCL-229
RKO	ATCC	Cat# CRL-2577
LS174T	ATCC	Cat# CL-188
COLO-205	ATCC	Cat# CCL-222
SW-1116	ATCC	Cat# CCL-233
CT26	ATCC	Cat# CRL-2638
HCT-116R	This paper	N/A
HT29R	Denise et al., 2015	N/A

(*Continued on next page*)

Continued

REAGENT or RESOURCE	SOURCE	IDENTIFIER
$p53^{-/-}$ HCT-116	Provided by Prof. G. Russo	N/A
ΔSHMT1 HCT-116	Provided by. J. D. Rabinowitz	N/A
Experimental models: Organisms/strains		
28-34 days-old male BALB/C mice	Charles River	Cat# 028BALB/C
4 weeks-old Foxn1nu/ nuAthymic nude mice	Envigo	Cat# 408761
Oligonucleotides		
siPHGDH	Thermo Fisher Scientific	Cat# AM16708, ID:108071, Lot# AS029NLH
siSHMT2	Thermo Fisher Scientific	Cat# AM16708, ID: 111555, Lot#AS02CWN2
siSHMT2	Thermo Fisher Scientific	Cat# AM16708, ID: 111555, Lot# AS02D727
Negative control-1	Thermo Fisher Scientific	Cat# AM4611
Negative control-2	Thermo Fisher Scientific	Cat# AM4613
TYMS-FW: 5′-CGGTGT GCCTTTCAACATC-3′	Thermo Fisher Scientific	N/A
TYMS-RV: 5′-TGTGCATC TCCCAAAGTGTG-3′	Thermo Fisher Scientific	N/A
PHGHD-FW: 5′-ATCTCTC ACGGGGGTTGTG-3′	Thermo Fisher Scientific	N/A
PHGHD-RV: 5′-AGGCTCG CATCAGTGTCC-3′	Thermo Fisher Scientific	N/A
PSAT1-FW: 5′-ACTTCCTGT CCAAGCCAGTGGA-3′	Thermo Fisher Scientific	N/A
PSAT1-RV: 5′-CTGCACCTT GTATTCCAGGACC-3′	Thermo Fisher Scientific	N/A
PSPH-FW: 5′-GAGCGGAC TCCCTTTTAAGC-3′	Thermo Fisher Scientific	N/A
PSPH-RV: 5′-CAGGGAG GTGAGCTGTGC-3′	Thermo Fisher Scientific	N/A
SHMT1-FW: 5′-TCCCGAGG ACTTTTGGAAGA-3′	Thermo Fisher Scientific	N/A
SHMT1-RV: 5′-TGCCACAG CACTCTGCATCT-3′	Thermo Fisher Scientific	N/A
SHMT2-FW: 5′-GCTCAACC TGGCACTGACTG-3′	Thermo Fisher Scientific	N/A
SHMT2-RV: 5′-CACTGATG TGGGCCATGTCT-3′	Thermo Fisher Scientific	N/A
SFXN1-FW: 5′-TCCTTCAAT GCCGTCGTCAA-3′	Thermo Fisher Scientific	N/A
SFXN1-RV: 5′-AGTGGTGAGA CATGCTTGGT-3′	Thermo Fisher Scientific	N/A
SLC1A4-FW: 5′-TGTGGTTGCA GCTTTCCGTACG-3′	Thermo Fisher Scientific	N/A
SLC1A4-RV: 5′-CCAGAGCAA ACAGGACCAATCC-3′	Thermo Fisher Scientific	N/A
SLC6A14-FW: 5′-ATCGTCTG GCAAGGTGGTAT-3′	Thermo Fisher Scientific	N/A
SLC6A14-RV: 5′-TGAGTGGCA GCATCTTTCCAT-3′	Thermo Fisher Scientific	N/A
GLDC-FW: 5′-GCCACCGC CACCGCCACCGC-3′	Thermo Fisher Scientific	N/A

(*Continued on next page*)

Continued

REAGENT or RESOURCE	SOURCE	IDENTIFIER
GLDC-RV: 5′-GAGCGAG CTCGCTTTCAAGC-3′	Thermo Fisher Scientific	N/A
β2M-FW: 5′-AGTATGCC TGCCGTGTGAAC-3′	Thermo Fisher Scientific	N/A
β2M-RV: 5′-GCGGCATCT TCAAACCTCCA-3′	Thermo Fisher Scientific	N/A
Software and algorithms		
Prism v.8.0	GraphPad	https://www.graphpad.com/
ImageJ	Schneider et al.2012	https://imagej.nih.gov/ij/
CFX Maestro Software Real-Time PCR System	BioRad	https://www.bio-rad.com/category/qpcr-analysis-software
Thermo XCalibur Quan Browser software	Thermo Fisher Scientific	RRID: SCR_014593
MZ-mine	Okinawa Institute of Science and Technology (Japan); VTT (Finland); Syngenta	http://MZmine.sourceforge.net/
Seahorse Wave software	Agilent Technologies	RRID:SCR_014526
imaris 6.1.5 software	Bitplane	RRID:SCR_007370
Vevo Lab software	Fujifilm Visualsonics	https://www.visualsonics.com/resource/vevo-lab-software
BioRender	BioRender	RRID:SCR_018361
TCGAbiolinks	Bioconductor	https://bioconductor.org/packages/release/bioc/html/TCGAbiolinks.html
Metascape	Metascape	www.metascape.org
Morpheus	Broadinstitute	https://software.broadinstitute.org/morpheus/

RESOURCE AVAILABILITY

Lead contact

Further information and requests for resources and reagents should be directed to and will be fulfilled by the Lead Contact, Paolo Paoli (paolo.paoli@unifi.it).

Materials availability

5-FU resistant cell lines generated in this study was generated as described in (Denise et al., 2015) and collected at the Department of Experimental and Clinical Biomedical Sciences "Mario Serio" (University of Florence).

All unique/stable reagents generated in this study are available from the Lead Contact without restriction. Any additional information required to reanalyze the data reported in this paper is available from the lead contact upon request.

Data and code availability

- The mass spectrometry files supporting the current study have not been deposited in a public repository due to the lack of a commonly accepted and feasible metabolomics file repository but are available upon reasonable request from the lead contact.
- Original western blot images are available at https://data.mendeley.com/datasets/hzbdfyz367/1.
- All data reported in this paper will be shared by the lead contact upon request.
- This paper does not report original code.
- Any additional information required to reanalyze the data reported in this paper is available from the lead contact upon request.

EXPERIMENTAL MODEL AND SUBJECT DETAILS

Cell lines

Male colorectal carcinoma cells HCT-116, HCT8, CACO-2, DLD-1, LoVo, COLO-205, SW-1116 (male), female colorectal carcinoma cells HT29, LS174T, RKO colorectal carcinoma cells, and mouse colorectal carcinoma cells CT26 were obtained from ATCC and

were cultured in high glucose (4.5 g/L) Dulbecco's modified Eagle's medium (DMEM) (Merck Sigma #D5671) supplemented with 10% fetal bovine serum (EuroClone #ECS0180L), 1% penicillin and streptomycin (EuroClone #ECB3001D), and 2mM L-glutamine (Merck Sigma #G7513). Cells were routinely grown in DMEM in a humidified atmosphere with 5% CO2 at 37°C. All cell lines were confirmed to be mycoplasma-free by Mycoalert detection kit (Lonza).

HCT-116 and HT29 cells resistant to 5-FU (respectively referred to as "HCT-116R" and "HT29R") were selected by treating HCT-116 and HT29 cells with increasing concentrations of 5-FU (Merck Sigma #F6627) for six months. Specifically, HCT-116 and HT29 cells were grown in standard conditions and maintained under selection with increasing concentrations of 5-FU (from 1 to 20 μM, rising by 0.5 μM every week), as previously reported (Denise et al., 2015). During the selection process, cells were routinely confirmed to be mycoplasma-free by Mycoalert detection kit (Lonza). Cells were finally stabilized in the presence of 20 μM FU. The resistance to 5-FU was assessed by MTT dye assay and by measuring apoptosis in the presence of increasing concentrations of 5-FU. To ensure maintenance of resistance to 5-FU, selected clones were treated with 20 μM of 5-FU for 48h every 15 days and let recover for one week before performing each experiment. HCT-116ΔSHMT1 were kindly provided by prof. J. D. Rabinowitz. p53−/− HCT-116 cells were a kind gift from Prof. G. Russo (University of Naples, Federico II).

Mouse models

All animal experiments were approved by the local authorities in accordance with all relevant ethical regulations. Housing and experimental animal procedures were approved by the Italian ethical committee of Animal Welfare Office of Italian Work Ministry (authorization number: 311/2022-PR). Mice were randomized before cancer cells injection and all samples were analyzed blinded. Sample size was determined using G power software in compliance with the 3R system: Replacement, Reduction, Refinement.

Housing and animal experiments were performed in accordance with national guidelines, approved by Italian ethical committee of Animal Welfare Office of Italian Work Ministry, and conformed to the legal mandates and Italian guidelines for the care and maintenance of laboratory animals.

For syngeneic experimental model, CT26 cells were implanted by bilateral subcutaneous injections (1×10^5 cells per flank in 100 μL PBS) into 36 three-weeks old Balb/c male mice (Charles River, UK). BALB/c mice were housed in filter top cages in a room maintained under a 12:12-h light:dark cycle, a temperature range of 20–24°C, and a humidity range of 30–70%.

For experiments with immunodeficient mice, HT29R cells were inoculated by bilateral subcutaneous injections (1×10^6 cells per flank in 100 μL PBS) into 24 three-weeks old Foxn1nu/nuAthymic nude male mice (Envigo RMS, USA). Nude mice were housed in autoclaved filter top cages in a positive pressure room under a 12:12-h light:dark cycle, a temperature range of 20–24°C, and a humidity range of 30–70%. Mice were provided with irradiated rodent chow and autoclaved tap water.

Mice were maintained on standard diet (Mucedola, Italy) and water ad libitum, and monitored daily until measurable tumors had formed. Tumor-bearing mice were then placed on experimental conditions and tumors were measured three times per week with calipers. Average tumor volume was calculated using the formula: $volume = \frac{length \times width^2}{2}$.

For the serine/glycine deprivation experiment, tumor-bearing mice were fed with a control or serine/glycine-free diet (50g/mouse/week) when measurable tumors had formed. Two days after diet change, mice were treated with vehicle (PBS, 5% ethanol) or 5-FU (40 mg/kg in PBS, 5% ethanol) with a cyclic regimen composed of three daily injections followed by two recovery days. 5-FU doses were adjusted to mouse weight with an injection volume of a maximum of 100 μL. The experimental diets applied were provided from (Mucedola, Italy) and were formulated as previously described as "Diet 1-Control" and "Diet 1-SG-free" in (Maddocks et al., 2017). Briefly, the control diet contains all the essential amino acids, including serine, glycine, glutamine, arginine, cystine and tyrosine. The serine/glycine-free diet has the same formulation of the control diet but lacks serine and glycine, compensated by a proportional addition of the other amino acids to reach an equal amount of amino acid content.

For NCT-503 experiment, tumor-bearing mice were treated with vehicle or NCT-503 (DivBio Science #S8619) (40 mg/kg) with IP injection daily starting from the day of measurable tumors formation. 5-FU-treated mice were injected with vehicle (PBS, 5% ethanol) or 5-FU (40 mg/kg in PBS, 5% ethanol) with a cyclic regimen composed of three daily injections followed by two recovery days. NCT-503 was prepared in a vehicle of 5% ethanol, 35% Kollisolv PEG E300 (Merck Sigma #91462), and 60% of an aqueous 30% hydroxypropyl-β-cyclodextrin (Merck Sigma #H107) solution. NCT-503 and 5-FU doses were adjusted to mouse weight with an injection volume of a maximum of 100 μL.

Humane endpoints were determined according to the parameters indicated in the project authorized by the Italian ethical committee of Animal Welfare Office of Italian Work Ministry (authorization number: 311/2022-PR).

METHOD DETAILS

Protein extraction and Western blot analysis

Cells were lysed in RIPA lysis buffer (50 mM Tris-HCl pH 7.5, 150 mM NaCl, 100 mM NaF, 2 mM EGTA, 1% Triton X-100) supplemented with protease (Merck Sigma #P8340) and phosphatase (Merck Sigma #P5726) inhibitors. Protein lysates were centrifuged at 14,000 rpm and 4°C for 10 min. Frozen tissue samples were fragmented to facilitate the lysis and resuspended in RIPA lysis buffer.

Cytoplasmic and nuclear lysates were separated by resuspending cells in a hypotonic cold solution (10 mM HEPES pH 8, 10 mM KCl, 1.5 mM MgCl, 1mM DTT, 0.1 mM EDTA, 0.2% NP40). The whole cell lysate was then centrifuged at 16000g for 10 min at 4°C ensuring the separations of the two fractions.

Extracted proteins were quantified using a bicinchoninic acid (BCA) assay (Merck Sigma #BCA1). Subsequently, 20–25 μg of total proteins were loaded on SDS-PAGE gels and transferred to PVDF membranes (BioRad #1704157). Membranes were incubated for 1h at room temperature in blocking buffer (5% non-fat dry milk (SantaCruz Biotechnology #sc-2325) in PBS-Tween 0.1%), and then incubated at 4°C over-night with primary antibodies (against either PHGDH (Thermo Fisher Scientific #PA5-54360), NRF2 (Genetex #GTX103322), phospho-H2AX (Abcam #81299), H3 (Cell Signaling #9715), p53 (SantaCruz Biotecnology #sc-126), p21 (SantaCruz Biotecnology #sc-271610), MDM2 (SantaCruz Biotecnology #sc-965), tubulin (SantaCruz Biotecnology #sc-5286), GAPDH (SantaCruz Biotecnology #sc-48166), β-Actin (Santa Cruz Biotechology #sc-47778). All primary antibodies were diluted 1:1000 in PBS-Tween 0.1% containing 5% BSA (Merck Sigma #A7906)). The following day, after washing in PBS-Tween 0.1%, membranes were incubated for 1h at room temperature with horseradish peroxidase-conjugated anti-mouse (Santa Cruz Biotechology #sc-2005) or anti-rabbit (Santa Cruz Biotechology #sc-2357) (diluted 1:2500 in PBS-Tween 0.1% containing 1% BSA) antibodies. Bound antibodies were detected using Clarity Western ECL Substrate (BioRad #1705061) and images were acquired using Amersham Imager 600 luminometer (Amersham, Buckinghamshire, UK). Quantification of bands was carried out by using the Amersham quantification software. β-Actin was used as loading control of total protein lysates. β-Tubulin and H3 were used to assess correct cellular compartment separation and as loading control respectively for cytoplasmic and nuclear compartments. All Western blot images are representative of at least three independent experiments.

Real-Time PCR

Total RNA was purified from cells using the RNeasy Plus Mini Kit (Qiagen #74134) according to manufacturer's instructions. Total RNA was quantified at NanoDrop Microvolume Spectrophotometer and Fluorometer (Thermo Fisher Scientific). Strands of cDNA were synthesized from 1 μg of total extracted RNA using the QuantiTect cDNA Reverse Transcription Kit (Qiagen #205311) and the MJ Mini Personal Thermal Cycler (Bio-Rad), according to manufacturer's instructions. Quantification of mRNA expression levels of specific targets was evaluated by Real Time PCR (RT-PCR) using QuantiFast SYBR Green PCR kit (Qiagen #204054). All the amplifications were run on CFX96TM Touch Real-Time PCR Detection System (Bio-Rad) according to the manufacturer's instructions. Data were reported as relative quantity with respect to the reference sample using the $2^{-\Delta\Delta Ct}$ method. β2 microglobulin (β2M) was used to normalize the data. The specific primers for mRNA analysis were provided from Thermo Fisher Scientific. The nucleotide sequences of the specific primers used are:

TYMS ((forward) 5′CGGTGTGCCTTTCAACATC-3′, (reverse) 5′TGTGCATCTCCCAAAGTGTG-3′); **PHGHD** ((forward) 5′ATCTC TCACGGGGGTTGTG-3′, (reverse) 5′AGGCTCGCATCAGTGTCC-3′); **PSAT1** ((forward) 5′ACTTCCTGTCCAAGCCAGTGGA-3′, (reverse) 5′-CTGCACCTTGTATTCCAGGACC-3′); **PSPH** ((forward) 5′-GAGCGGACTCCCTTTTAAGC-3′, (reverse) 5′-CAGGGAGGT GAGCTGTGC-3′); **SHMT1** ((forward) 5′TCCCGAGGACTTTTGGAAGA-3′, (reverse) 5′-TGCCACAGCACTCTGCATCT-3′); **SHMT2** ((forward) 5′-GCTCAACCTGGCACTGACTG-3′, (reverse) 5′CACTGATGTGGGCCATGTCT-3′); S**FXN1** ((forward) 5′TCCTTCA ATGCCGTCGTCAA-3′, (reverse) 5′AGTGGTGAGACATGCTTGGT-3′); S**LC1A4** ((forward) 5′TGTGGTTGCAGCTTTCCGTACG-3′, (reverse) 5′CCAGAGCAAACAGGACCAATCC-3′); S**LC6A14** ((forward) 5′ATCGTCTGGCAAGGTGGTAT-3′, (reverse) 5′TGAGTGG CAGCATCTTTCCAT-3′); G**LDC** ((forward) 5′-GCCACCGCCACCGCCACCGC-3′, (reverse) 5′GAGCGAGCTCGCTTTCAAGC-3′). **β2M** ((forward) 5′AGTATGCCTGCCGTGTGAAC-3′, (reverse) 5′-GCGGCATCTTCAAACCTCCA-3′).

RNAi transfection

Cells were transfected with 20 nmol/L PHGDH (Thermo Fisher Scientific, Cat# AM16708, ID:108,071, Lot#AS029NLH) or SHMT2 (Thermo Fisher Scientific, Cat#AM16708, ID: 111,555, Lot#AS02CWN2; Thermo Fisher Scientific, Cat#AM16708, ID: 111,555, Lot#AS02D727) siRNA silencers and respective Silencer Select Negative Control (Thermo Fisher Scientific Cat #AM4611.

Cat#AM4613) using Lipofectamine RNAiMAX Reagent (Thermo Fisher Scientific #13778-150) and Opti-MEM (GIBCO #31985062) according to manufacturer's instructions. The silencing efficacy was assessed following 24h, 48h and 72h after the transfection by both real-time and Western blot analysis. Following experiments were performed 48h after transfection.

Viability assay

3×10^4 cells were seeded in 24-well plates and treated 24 h later with either standard conditions (see cell culture) or experimental conditions as previously described. 48h after the treatment, cells were washed with PBS (Merck Sigma #D8537) and stained with crystal violet (triphenylmethane dye 4-[(4-dimethylaminophenyl)-phenyl-methyl]-N,N-dymethyl-alanine; Merck Sigma #548629) in 20% methanol solution for 30 min at room temperature. Plates were let dry overnight and the crystal violet within the adherent cells was solubilized with 200 μL/well of 2% SDS. The absorbance at 595 nm was measured using a spectrophotometer (Microplate Reader 550, BioRad). Hypoxanthine (#H9377), Lometroxol hydrate (#SML-0040), NCT-503 (#SML-1659), Pemetrexed (#SML1490), and Thymidine (#T1895) used in viability assays were provided by Merck Sigma.

Proliferation assay

1.5-2×10^5 cells/well were seeded in standard medium in six-well plates and allowed to adhere for 24h. Triplicate wells were seeded for each experimental condition, including "time zero" to calculate relative cell numbers. Standard medium was substituted by experimental media at the "time zero" of each experiment. At each time point, cells were trypsinized (Trypsin EDTA, EuroClone #ECM0920D), resuspended in standard DMEM, and counted.

Experimental media were formulated starting from MEM medium (Gibco #21090) supplemented with 10% dialyzed FBS, 1% MEM vitamins (Merck Sigma #M6895), 2 mM L-glutamine (Merck Sigma), D-glucose (Merck Sigma #G8644) to reach a final concentration 17 mM, 1% penicillin and streptomycin (EuroClone #ECB3001D), and 2mM L-glutamine (Merck Sigma #G7513). To generate *"+ser + gly" media*, 0.4mM serine (Merck Sigma #S5386) and 0.4 mM glycine (Merck Sigma #G8790) were added;*"-ser -gly" media* lack these two amino acids.

Colony forming assay

After 24 h of treatment with 5-FU at the indicated concentrations, 1 × 10^3 cells were seeded into six-well plates and cultured for 9–11 days. Cells were then fixed and stained with an aqueous solution containing 1% crystal violet and 10% methanol. Colonies were photographed and counted using the ImageJ imaging system. The number of colonies formed after incubation was calculated as a surviving fraction (SF): $SF = \frac{n\ of\ colonies\ formed\ after\ incubation}{n\ of\ cells\ seeded \times PE}$ where PE indicates the Plating Efficiency, calculated in untreated cells as the ratio of the colonies number and the number of seeded cells (Franken et al., 2006).

Radioactive assays

Serine up-take assay

2× 10^5 cells/well cells were plated in six-well plates in triplicate wells in their regular medium and let to adhere for 24h; duplicate plates were seeded for normalization by cell counting. Exogenous serine uptake was evaluated by incubating cells in a serum starved medium with serine substituted for [1-2^{14}C]-serine for 15 min. Cells were subsequently washed twice with PBS, and lysed with 0.1 mol/L NaOH. Cell lysates were transferred to a scintillation vial and measured on the scintillation counter (Tri-Carb 2800TR, PerkinElmer). The radioactive signals were normalized to cell number.

CO_2 production

2× 10^5 cells/well cells were plated in six-well plates in triplicate wells in their regular medium and let to adhere for 24h; duplicate plates were seeded for cell counting. The standard medium was than replaced with a medium where serine was substituted for [1-2^{14}C]-serine (for exogenous serine uptake assay) or [1-^{14}C]-glucose and [6-^{14}C]-glucose (for PPP activity assay), and cells were incubated for 15 min at 37°C. Each plate was covered with a section of Whatman paper facing the inside of the dish wetted with 100 μL of phenyl-ethylamine-methanol (1:1) to trap CO_2. 200 μL of 4M H_2SO_4 was then added and cells were incubated at 37°C for the following 1 h to allow the release of $^{14}CO_2$. Finally, Whatman paper was removed and put into scintillation vials for counting. The amount of $^{14}CO_2$ trapped in the paper dishes was measured using a liquid scintillator analyzer (Tri-Carb 2800TR, PerkinElmer). The radioactive signals were normalized to cell number.

Liquid chromatography–mass spectrometry (LC–MS)

HCT-116 and HCT-116R cells (2 × 10^5 cells/well) were seeded in six-well plates in triplicate wells in their regular medium; duplicate plates were seeded for cell counting. After 24h growth in the stated conditions metabolites were extracted. For isotopomer distribution assays, media containing [U-^{13}C]-glucose (final concentration 17mM) or [U-^{13}C]-serine (final concentration 0.4 mM) was added before metabolite extraction at different time points (30min, 1h, 3h for [U-^{13}C]-glucose experiments, and 3h, 8h, 24h for [U-^{13}C]-serine experiments). Labeled media was formulated starting from MEM medium (Gibco #21090) supplemented with 10% dialyzed FBS, 1% MEM vitamins (Merck Sigma #M6895), 1% penicillin and streptomycin (EuroClone #ECB3001D), 2mM L-glutamine (Merck Sigma #G7513), 0.4 mM glycine (Merck Sigma #G8790). 0.4 mM serine (Merck Sigma #S5386) was added to ^{13}C-glucose labeled media; D-glucose (Merck Sigma #G8644) to reach a final concentration 17 mM was added to ^{13}C-serine labeled media.

Metabolites were extracted by lysing cells in a cold (−20°C) solution of methanol/acetonitrile/H_2O (50:30:20). Samples were shaken at 4°C for 10 min, then centrifuged for 15 min at 16,000 × g. The supernatant was then collected and analyzed by LC-MS. Analytes were separated using hydrophilic interaction liquid chromatography with a SeQuant ZIC-pHILIC column (2.1 × 150 mm, 5 μm) (Merck) and detected with high-resolution, accurate-mass mass spectrometry using an Orbitrap Exactive in line with an Accela autosampler.

Gas chromatography-mass spectrometry (GC–MS)

2 × 10^5 cells/well were seeded in six-well plates in triplicate wells in standard medium. Cells were let to adhere for 24h and then metabolites were extracted. For isotopomer distribution assays, fresh media containing [U-^{13}C] serine and formulated as described before (see Liquid chromatography–mass spectrometry (LC–MS) section) was added 24h before metabolite extraction.

Metabolites from cells were extracted by quenching plates in liquid nitrogen to arrest metabolic processes, and lysing cells in 800 μL of a cold (−20°C) solution of methanol 80% in water (containing 0.75 μg norvaline/sample as internal standard) and

500 μL chloroform. Metabolites from culture media were extracted by adding 50 μL of cold solution of methanol 80% in water (containing 0.75 μg norvaline/sample as internal standard) to 50 μL of media previously centrifuged for 10 min at 1.000 rpm. Metabolites from plasma were extracted by adding 100 μL of cold solution of methanol 80% in water (containing 0.75 μg norvaline/sample as internal standard) and 100 ul of chloroform to 100 ul of plasma. Plasma was isolated from blood samples quickly collected via cardiac puncture in heparin-containing tubes by centrifuging for 15 min at 2.500 rpm. Metabolites from tissues were extracted by resuspending mashed tissue fractions (50–70 mg) in 400 μL of cold solution of methanol 50% in water and 400 μL of chloroform, and sonicating them three times (10 s each). Tissue for metabolites extraction were rapidly dissected, washed in ice-cold saline, frozen in liquid-nitrogen, and samples were stored at −80°C until processing. Samples were vortexed at for 10 at 4°C minutes and then centrifuged at 4°C and 14.000 rpm for 10 min. Centrifuging results in a three phases separation: polar metabolites in the upper water/methanol phase, protein layer in the middle position, fatty acids in the lower chloroform phase. Polar metabolites were derivatized with 30 μL of a solution 20 ug/ml methoxyamine (Merck Sigma #226904) in pyridine (Merck Sigma #270970) for 90 min at 37°C. Then, 45 ul of N-(tert-butyldimethylsilyl)-N-methyl-trifluoroacetamide, with 1% tert-butyldimethylchlorosilane (Merck Sigma #375934) were added in each sample and incubated for 60 min at 37°C. GC-MS runs were with helium as carrier gas with a flow rate of 0.6mL/min. The split inlet temperature was set to 250°C and the injection volume of 1μL. The GC oven temperature ramp was from 70 to 280°C. The first temperature ramp was from 70 to 140°C at 3°C/min. The second temperature ramp was from 140 to 180°C at 1°C/min. Finally, the latest temperature ramp was from 180 to 280°C at 3°C/min. For the Quadrupole, an EI source (70eV) was used. The ion source and transfer line temperatures were set, respectively, to 250 and 290°C. For the determination of relative metabolite abundances, the integrated signal of all ions for each metabolite fragment was normalized by the signal from norvaline and sample protein content isolated by resuspending the protein layer in 50 μL NaOH 200 mM, vertexing for 15 min at 96°C, and centrifuging at 4°C 14.000rpm for 15 min. Protein abundance was measured by BCA assay. For labeling experiments, the measured distributions of mass isotopomers were corrected for natural abundance of ^{13}C using IsoCor software (Millard et al., 2019) and the abundance of each isotopologue is indicated as normalized to the sum of all possible isotopologues (Buescher et al., 2015).

Cytosolic and mitochondrial fractions isolation

Cytosolic and mitochondrial metabolites content were separated by permeabilizing cytosolic with digitonin as described in (Nonnenmacher et al., 2017, 2019) 2×10^5 cells/well were seeded in a 6-well plate in standard medium and let to adhere for 24h. Fresh media containing [U-^{13}C] serine was added 24h before metabolite extraction. Labeled media was formulated starting from MEM medium (Gibco #21090) supplemented with 10% dialyzed FBS, 1% MEM vitamins (Merck Sigma #M6895), 1% penicillin and streptomycin (EuroClone #ECB3001D), 2mM L-glutamine (Merck Sigma #G7513), D-glucose (Merck Sigma #G8644) to reach a final concentration 17 mM, and 0.4 mM glycine (Merck Sigma #G8790). Cells were then washed and incubated with 500 μL digitonin solution (40 μg/mL in mitochondrial assay buffer) for 2 min at 37°C to selectively permeabilize the cytosolic membrane. Supernatants containing the cytosolic components were collected and stored at −80°C (Rinaldi et al., 2021). The plates holding intact mitochondria were washed with a 0.9% NaCl solution, quenched in liquid nitrogen, and stored at −80°C. The supernatants containing cytosolic metabolites were dried in and metabolites were then extracted as described before for GC-MS analysis. Mitochondrial metabolite extraction was performed as previously described for GC-MS analysis.

Seahorse analysis

3×10^4 cells/well were seeded in XFe96 cell culture plates (6–8 technical replicates per condition) with 80 μL of standard medium and let to adhere at 37°C for 4-6h. Standard medium was then replaced with *"+ser + gly"* or *"-ser-gly"* (see Proliferation assay section) for the following 16h. 1h before the analysis, media were replaced with *"+ser + gly"* or *"-ser-gly"* with adjusted PH at 7.4. Cells were incubated for 1h at 37°C in atmospheric CO_2 conditions to pre-equilibrate cells. OCR and ECAR analysis were performed using Seahorse XF Cell Mito Stress Test (Agilent # 103,015-100) according to manufacturer's instructions. Mitochondrial drugs were utilized as follows: 0.8 μM of oligomycin, 1 μM of FCCP, 1 μM of rotenone, and 1 μM of antimycin A were injected three times subsequently at the times indicated. Results were normalized to protein content. Basal respiration is calculated as the average rate measurement before injection minus the average of non-mitochondrial respiration rate. Maximal respiration is calculated as the average of the maximum rate measurement after FCCP injection minus the average of non-mitochondrial respiration.

Intracellular ATP quantification

ATP levels were determined using the ATP detection kit-luminescence assay kit (CAY-700410-1-BioVision, milpitas, CA) according to the manufacturer's instructions. All data were normalized on cell protein content

Confocal microscopy image acquisition

Cells were stained with 200 nM TMRE probe (T669, Thermo Fisher Scientific) for 20 min at 37°C and examined using a confocal microscope (TCS SP8; Leica, Wetzlar, Germany). 1μg/ml Hoechst (62,249, Thermo Fisher Scientific) was used to visualize the nuclei. 3D reconstruction was assessed using Leica LasX 3D software. Mitochondrial abundance was quantified as the mean mitochondrial surface. The analysis was performed with the imaris 6.1.5 (Bitplane) software using the "highlights surfaces" algorithm. The external surface of each mitochondrion was calculated and reported as the average mitochondrial surface for each image.

In vivo ultrasound imaging

Ultrasound (US) imaging was carried out at Laboratory of Genetic Engineering for the production of Animal Models (LIGeMA) at the Animal Facility of the University of Florence. US imaging were performed to evaluate the tumor development with Vevo LAZR-X (Fujifilm Visualsonics) platform. Axial 3D scans of the tumors were performed in B-Mode by using a 55-MHz transducer. During the procedure mice were anesthetized by isoflurane (2%) and placed on a heated pad at 37°C in prone position. Respiration rate, ECG, and body temperature were monitored during the procedure. Tumor volumes were analyzed by using Vevo Lab software (Fujifilm Visualsonics). The volumes were measured delineating the ROI (Region Of Interest) for every axial slide using Vevo LAB software.

TCGA-COADREAD dataset analysis

Data from The Cancer Genome Atlas (TCGA) consortium (Database: TCGA; http://firebrowse.org) were retrieved and the Colorectal Adenocarcinomas (COADREAD) IlluminaHiSeq and/or Illuminaga mRNA expression profiles enquired only for patients whose response to 5-FU treatment was available (n = 338). The follow-up to 5FU treatment was used to cluster patients in Responder (R) and Non-Responder (NR) subgroups further tested by overall survival analysis (Figure S5A). Differential expressed genes (DEGs) were then evaluated on the whole dataset or after dividing it into subtypes according to Consensus Molecular Subtypes (CMS) classification (Guinney et al., 2015). DEGs were selected by using Mann–Whitney U test. The statistical analyses were conducted with TCGA biolinks (Silva et al., 2016) in the R Studio Bioconductor environment. In order to recognize the effects of the 5-FU resistance on metabolic rewiring, we filtered DEGs with the mammalian metabolic enzyme list, a catalog of genes/enzymes involved in metabolic processes and based on the Mitocarta database (Pagliarini et al., 2008), as described by Corcoran et al., 2017) (Corcoran et al., 2017). Pathway analysis of DEGs was performed on www.metascape.org as described by Zhou et al. (Zhou et al., 2019). Briefly, after the upload of the multiple gene identifiers, the list of metabolic DEGs was compared to thousands of gene sets, including GO processes, KEGG pathways, Reactome gene sets, canonical pathways, CORUM complexes, and MSigDB, to define their involvement in specific biological processes. Gene sets whose members were significantly overrepresented were reported as putative biological discoveries, while ontology terms and interactome networks that did not meet the minimal statistical requirements were removed.

QUANTIFICATION AND STATISTICAL ANALYSIS

Statistical data analysis was performed with GraphPad Prism version 8.0 (GraphPad Software) on at least three biological replicates for each experiment. Details on statistical tests and post-tests are presented in the figure legends. Sample size for all experiments was chosen empirically. Independent experiments were pooled and analyzed together whenever possible as indicated in figure legends. Data are presented as mean ± SEM., as indicated in the figure legends. Mathematical outliers were detected using Grubb's test (alpha = 0.1) and values identified were removed.